APPLICATIONS OF COMBINED EXTINCTION/ABSORPTION SPECTROSCOPY – DAIRY ANALYSIS, MICROPLASTICS STUDY, AND VITAMIN ASSESSMENT

Phuong Bui

Supervised by Eric Le Ru

Master Thesis

School of Chemical and Physical Sciences

Victoria University of Wellington

February 2022

TABLE OF CONTENTS

TABLE OF FIGURES

ABSTRACT

Combined extinction/absorption spectroscopy is the combination of conventional ultraviolet and visible spectroscopy (UV Vis Spectroscopy) and diffuse-light absorption spectroscopy, i.e. using an integrating sphere (IS), in one instrument. The combination provides two optical properties of the sample in one trial, i.e. extinction and absorption. Scattering is computed by subtracting absorption from extinction. Hence, we obtain three UV Vis spectra of the sample in one measurement – extinction, absorption, and scattering. This information is important to understand the optical behavior of the sample or its interaction with UV Vis radiation. In addition, the integrating sphere could provide information of turbid media through its absolute absorption spectra when scattering is a matter. It is promising in real-time analyzing practical samples such as waste water, bio-fluid, or food.

This research aims to apply combined extinction/absorption spectroscopy into investigating the optical properties of materials – absorption and scattering, as well as chemical information of turbid samples through the absolute absorbance that could not be studied by a standard UV Vis spectrometer. It is promising for practical samples in environment, food, and biomedicine because most of them are too cloudy to be measured directly by a conventional setup. Three projects are run – microplastics study, dairy analysis, and vitamin assessment.

In dairy analysis, it showed peaks of nutrients – fat, protein, vitamin A, vitamin B2, and beta-carotene in a number of milk types and cream. In addition, the Lambert-Beer lines are constructed for fat and protein content in milk and cream. Preliminarily, they are linear in low concentration and non-linear in higher ones. Some hypotheses are raised to explain these phenomena.

In microplastics study, commercial latex sphere polystyrene samples with different diameters are measured and their optical properties or UV Vis spectra are harvested – extinction, absorption, and scattering. One investigation that has not been reported yet is their absorption in UV range shown by comparing with their electromagnetic models.

In vitamin assessment, dissolution study of complex vitamin B and vitamin C effervescent tablet showed real-time release of active agents by the absorption spectra.

CHAPTER 1 – COMBINED EXTINCTION/ ABSORPTION SPECTROSCOPY

1.1. Ultraviolet and visible Spectroscopy (Extinction spectroscopy)

Spectrometer: A standard ultraviolet and visible spectrometer includes ultraviolet and visible sources - normally two lamps, one for ultraviolet radiation and one for visible radiation, the monochromator system, a sample holder, and a detector. Figure 1 shows the schematic of a conventional ultraviolet and visible spectrometer.

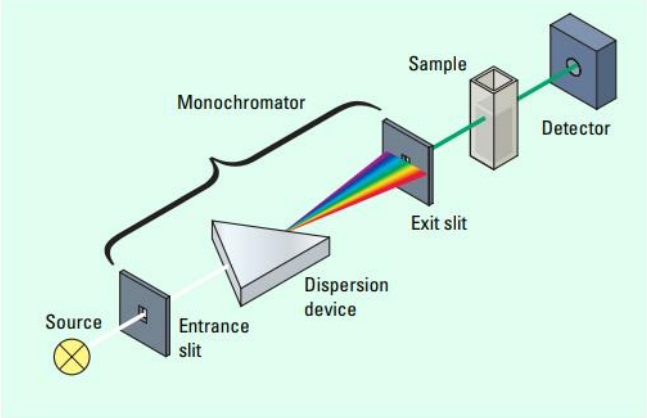

Figure 1: Schematic of a conventional ultraviolet and visible spectrometer [1].

Basic principle: Ultraviolet (UV) and visible (Vis) radiation are parts of the electromagnetic spectrum. They have spectral range of 100-400 nm and 400-700 nm, respectively and their energy can be calculated by the equation E = hv, where h is the Planck's constant ($6.62607004 \times 10^{-34}$ m^2 kg /s) and v is the frequency of the radiation. Figure 2 illustrates the electromagnetic spectrum where the radiations are classified by their frequencies and wavelengths.

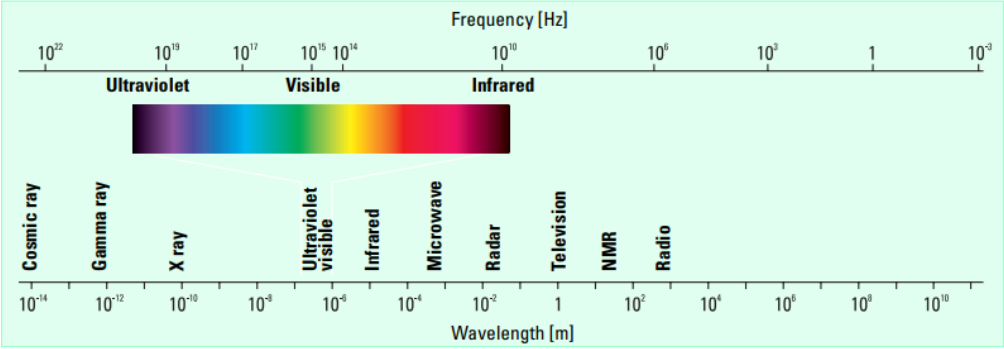

Figure 2: The electromagnetic spectrum [1].

When the radiation interacts with the matter, there is a number of processes that occur – reflection, scattering, absorption, fluorescence, and photochemical reaction. In UV Vis spectroscopy, we only want the absorption to happen. The absorption of light by matter increases the energy content of the atom or molecule and can cause the electronic transition(s) in those. The total energy of the particle equals to its electronic, vibrational, and rotational energy levels.

$$E_{total} = E_{electronic} + E_{vibrational} + E_{rotational}$$

In comparison with the atom, the molecule has its electronic energy levels superimpose on the vibrational and rotational energy levels. Therefore, when there are many transitions with different energy levels, its UV Vis spectrum is broader than that of the atom (shown in figure 3).

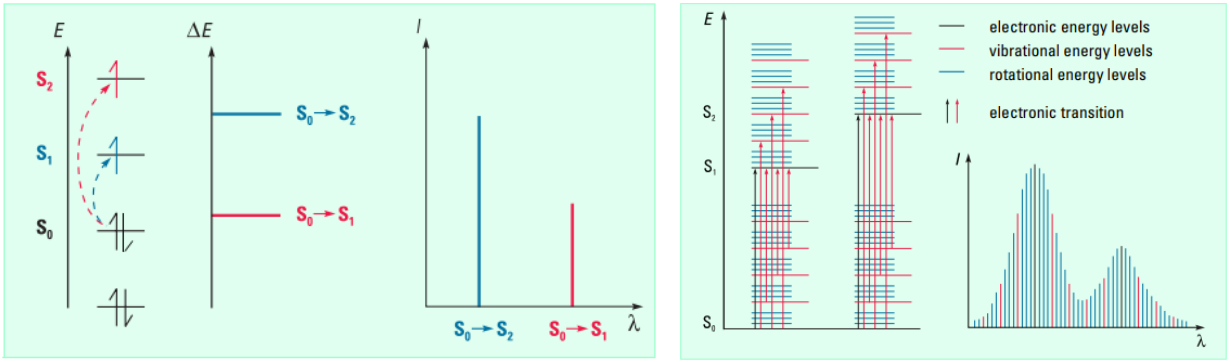

(a) (b)

Figure 3: Electronic transitions and UV Vis spectra (a) in atom, (b) in molecule [1].

For example, in formaldehyde, when it absorbs UV Vis light, there are two types of electronic transition that occur – moving of electrons from class n to class pi* at wavelength 285 nm and from class pi to class pi* at wavelength 187 nm (Figure 4).

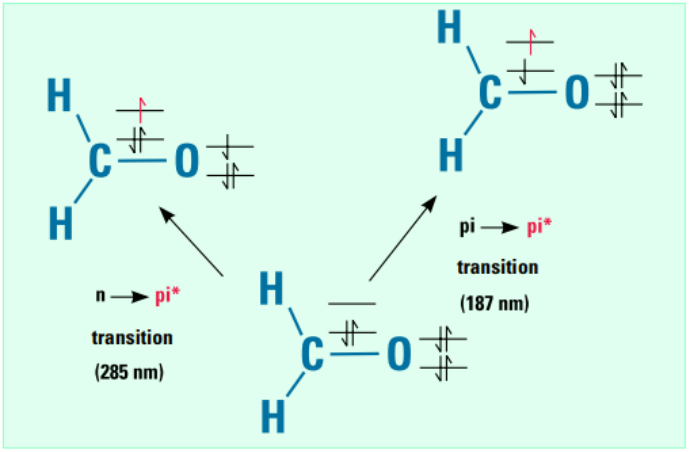

Figure 4: Electronic transitions in formaldehyde when interacts with UV Vis radiation [1].

Qualitative analysis: There are two parameters to evaluate the absorption of light by the particles - transmittance (T) and absorbance (A). $T = I/I_0$, where I_0 is the incident radiation and I is the transmitted radiation that passed through the sample. Whereas, A is defined by the equation $A = -\log_{10}T$.

The indicator of a substance by UV Vis spectroscopy is its absorbance maxima. For example, acetone (containing group ketone or RR'C=0) has its absorbance maxima at wavelength 271 nm while that of acetaldehyde (containing group aldehyde or RHC=0) is 293 nm. However, there are other factors that can affect this position such as the molecular environment, the solvent, pH, or the temperature.

Quantitative analysis: The concentration of the sample can be calculated by the Beer-Bouguer-Lambert law,

$$A = \varepsilon bc$$

, where A is the absorbance or optical density (OD), ε is the molar absorption or extinction coefficient, b is the path length, and c is the concentration of the sample.

Figure 5 describes the positive correlation between the absorbance of the sample with its concentration stated in the Beer-Bouguer-Lambert law.

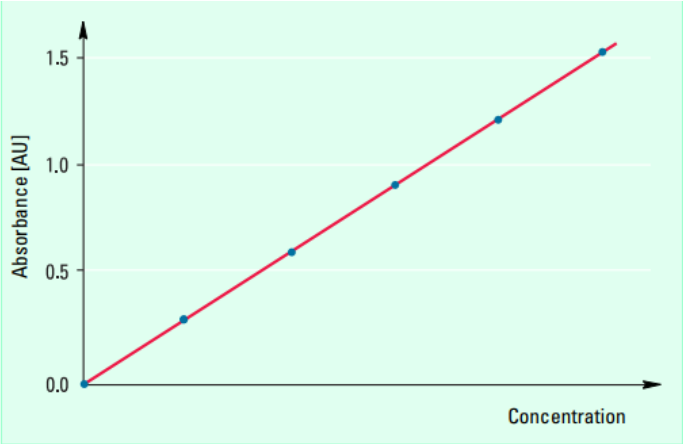

Figure 5: The Beer-Bouguer-Lambert law [1].

Extinction, absorption, & scattering: In an ultraviolet and visible spectrometer, there are two main physical phenomena, i.e. absorption and scattering. When the sample is illuminated by the electromagnetic wave, its electric charges, i.e. electrons and protons, are set into oscillatory motion. The accelerated electric charges will re-radiate the electromagnetic energy in all directions as the secondary radiation and this is called scattering while the excited elementary charges may transform part of the incident field into other forms such as thermal energy and it is known as the absorption [2].

In spectroscopy, the amount of photons which cannot reach the detector may come from both processes, scattering and absorption. We call this total the extinction.

$$\text{Extinction} = \text{Scattering} + \text{Absorption}$$

In samples with molecular scale, the main process is the absorption. Therefore, the extinction equals to the absorption. Whereas in nanoparticle samples, due to the large size of the particles which associates with the scattering effects, there are two processes – scattering and absorption [3]. Hence, the optical density is the extinction, sum of scattering and absorption, which cannot reflect accurately the concentration of the measured sample. Figure 6 describes the process happened in a standard UV Vis spectroscopy for nanoparticle samples. The incident light is both absorbed and scattered partly when passing through the sample which contributes to its reduction of intensity.

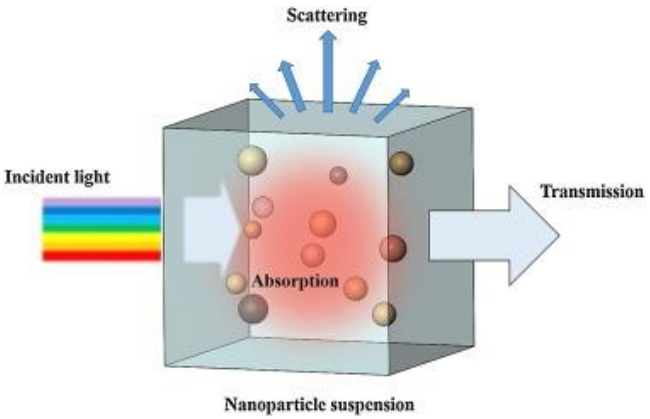

Figure 6: Absorption and scattering process for nanoparticle samples in a standard UV Vis spectroscopy [4].

In turbid medium, due to scattering effect, there may be no light passing through the sample for a standard UV Vis setup. That gives no chemical information about the measured sample.

Many techniques and methods have been developed to solve these scattering challenges in UV Vis spectroscopy. In this thesis, we will discuss about one of those techniques - the integrating sphere and its application in UV Vis spectroscopy for scattering-free absorption spectroscopy.

1.2. Integrating sphere (Absorption spectroscopy)

Theory: The integrating sphere (IS) is an instrument whose function is to integrate the radiant flux in its cavity. Figure 7 demonstrates a typical diagram of an integrating. The system consists of a light source, a sphere, a sample holder, and a spectrometer.

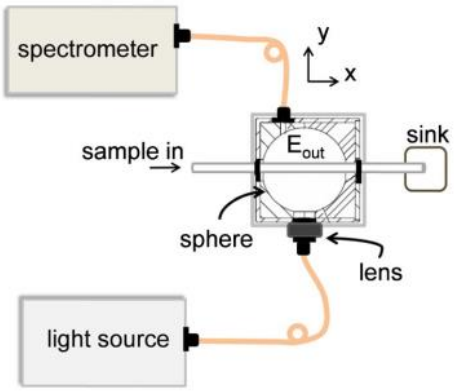

Figure 7: Diagram of an integrating sphere (IS) [5].

Theory of the integrating sphere is based on the property of the sphere cavity surface (that is diffuse reflecting surface or Lambertian surface) and the radiation exchange within an enclosure of diffuse surfaces [6].

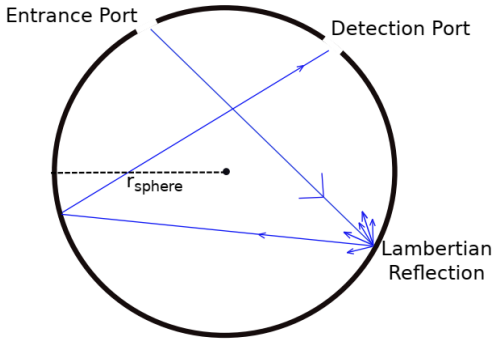

Figure 8: A typical integrating sphere [7].

Reflections from a Lambertian surface follow Lamberts cosine law whereas the observed projected area from the surface is also a cosine dependence. As a result, the reflected radiance becomes independent of the viewing angle. Which means the reflected radiance is the same for any angle.

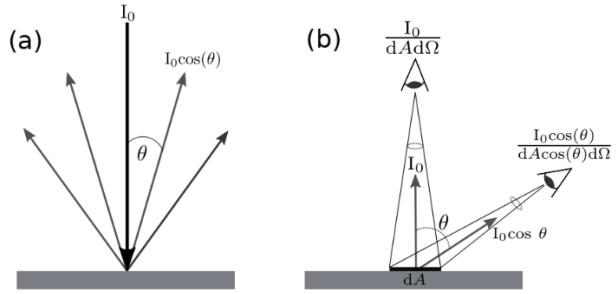

Figure 9: Reflections from a Lambertian surface, (a) the reflected intensity, (b) the projected area [7].

One of the most important equations for the integrating sphere is the integrating sphere radiance equation shown in the figure 10.

Radiance of diffuse surface — Sphere multiplier

$$L_S = \frac{\phi_i}{\pi A_S} \times \frac{\rho}{1-\rho(1-f)}$$

Figure 10: The integrating sphere radiance equation [6].

Where:

L_S is the sphere surface radiance

ϕ_i is the input flux

π is the total projected solid angle from the surface

A_S is the total cavity surface area of the sphere

ρ is the sphere surface reflectance

f is the port fraction

This equation is used to predict IS radiance for a given input flux as a function of sphere diameter, reflectance, and port fraction. As can be seen, there are two main parts in the equation. The first represents the radiance of the diffuse surface, strongly depending on a particular input flux. The second part is one of the most important sphere's parameter, i.e. the sphere multiplier.

For the sphere multiplier, it is the calculation for the increase in radiance when light reflects many times on the sphere surface and it strongly depend on both port fraction, f, and the sphere surface reflectance, ρ. The chart below illustrates the magnitude of the sphere multiplier. For most integrating sphere with 0.94<ρ<0.99 and 0.02<f<0.05, the sphere multiplier is in the range of 10-30 [6] (Figure 11).

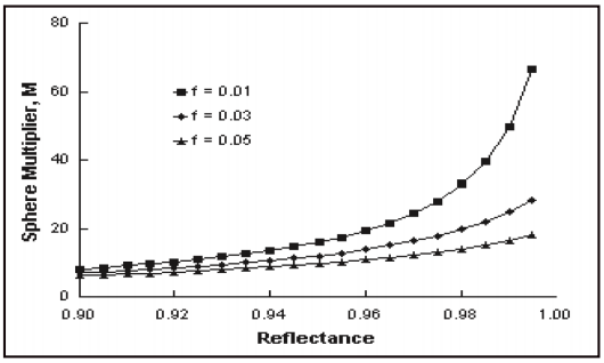

Figure 11: The magnitude of the sphere multiplier [6].

Applications: One of the applications of the integrating spheres is quantitative photometry, i.e. the measurement of how much power of light emitted. The oldest application for the integrating sphere is the measurement of total geometric luminous flux from electric lamps. Another application is quantum yield, that is how much light re-emit in fluorescence. Others are diffuse reflectance and transmittance and integrating-cavity absorption meter (ICAM). Figures 12 show the applications of the integrating spheres in photometer and measurement of reflectance and transmittance.

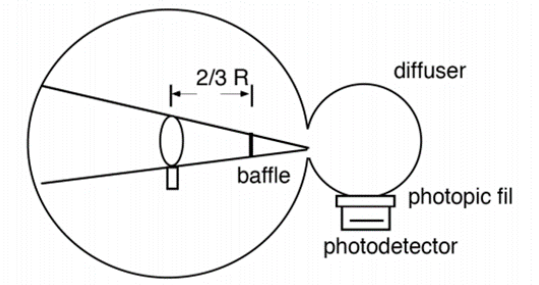

(a)

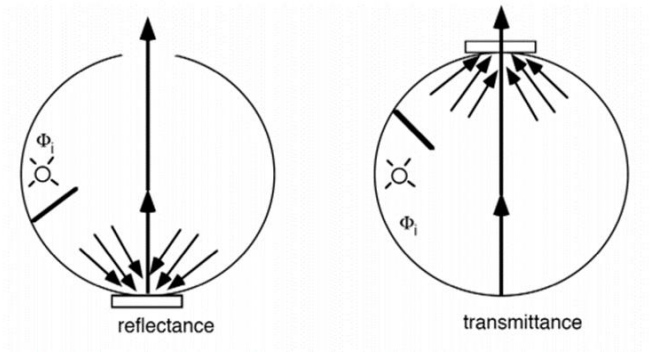

(b)

Figure 12: Applications of the integrating spheres, (a) Sphere photometer, and (b) Measurements of reflectance and transmittance of materials [6].

Absorption spectroscopy in an integrating sphere: Absorption is an important optical property of a sample. It can be used for both qualitative and quantitative analysis. However, scattering can affect the measurement if particles larger than ~5-10 nm are present. There have been attempts to solve this challenge, for example using photoacoustic spectroscopy, but integrating spheres arguably provide the most accessible solution. Its principle is the measurement of low absorption by the long path length (i.e. the effective path length) which comes from the high reflectivity of the cavity surface of the sphere [8]. The first setup idea was an Integrating Cavity Absorption Meter (ICAM), which measured the medium filling entirely the inside of the sphere, with a limitation to gas measurement due to the contamination or damage liquid could create to the cavity [6], [8], [9]. The idea of placing a container (typically a cuvette in the center of the sphere) has been raised since 1970 [10] but only had limited applications to the measurement of seawater in environmental studies such as aquatic particles or microalgae which strongly scattered light [11]–[14]. Recently, the setup gained new attention in plasmonics and nano-optics for measuring the optical properties of nanoparticles, in particular the interaction between visible light and silver nanoparticles in water, which contributes to the synthesis process of the particles [15] or the study of the absorption properties of dye adsorbed on metallic nanoparticles for surface-enhanced spectroscopy [16], [17]. Another recent utility of the setup is to measure protein concentration in turbid media which is useful in biotechnology due to the diverse applications of the protein-particle conjugates [18].

Figure 13 shows the schematic of a centrally mounted cuvette integrating sphere (CMCIS) setup utilized to measure the absolute absorbance of a sample. The system has a white light source, an entrance port, a cuvette holder, an exit port, and a spectrometer. During the measurement, radiation is randomly reflected by the sphere surface following the Lambertian cosine law, which means it becomes independent of the viewing angle. Light will pass through the samples several times, where it may be absorbed. If light is scattered, it simply finds its way back inside the sphere. Unabsorbed light is detected at a port on the wall of the sphere and can be related to the sample absorption, independent of any scattering [7].

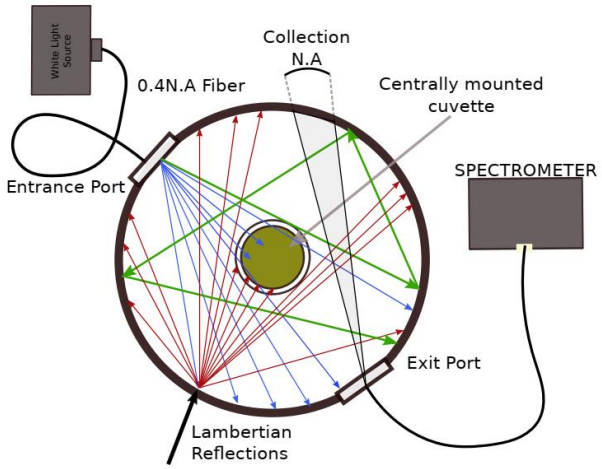

Figure 13: Schematic of the centrally mounted cuvette integrating sphere (CMCIS) setup utilized to measure the absorbance of the sample [7].

One of challenges for the scattering-free absorption measurement is the complicated propagation of light when it interacts with a sample inside an integrating sphere. Light can reflect randomly on the sphere wall and may go through the sample a number of times with random directions, which adds up to an effective pathlength through the sample A variety of methods have been developed to study this phenomenon and to perform calibration procedure which can correct the pathlength to achieve spectra in 1cm-equivalent pathlength optical density (OD) such as Monte-Carlo simulation [11], [19], [20], or semi-analytic models [5]. Figure 14 illustrates the propagation of photons in the integrating sphere from their first pass to the final when they reach the detector. In this simple example, we assume an empty sphere (as in an ICAM). For CMCIS, the presence of a sample complicates this analysis.

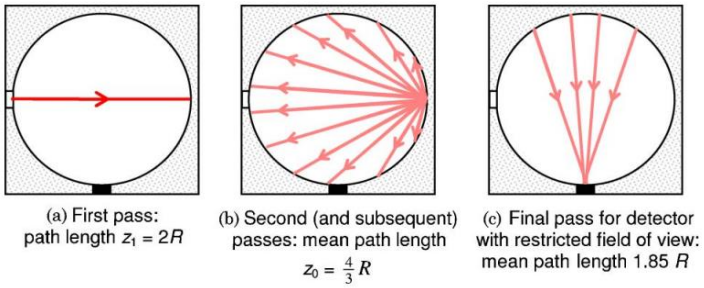

Figure 14: Full model for path-length distribution, the propagation of photons in the integrating sphere from their first pass to the final when they reach the detector [19].

1.3. The CloudSpec: an instrument implementing (Combined extinction/absorption spectroscopy)

Introduction: CloudSpec (commercialized by Marama Labs) shown in the Figure 15 is an instrument that integrates both functions of a conventional UV Vis spectrometer and an integrating sphere which can give two optical properties of a material at once – extinction and absorption. For the turbid sample, it still can provide the absorption spectrum using an integrating sphere based setup.

Figure 15: CloudSpec instrument [21]

Principle: CloudSpec implements the ICAM/CMCIS idea and a conventional transmission UV Vis measurement; hence, it can perform two measurements – extinction and absorption – in one trial. The process is shown in figure below. Light will pass through the sample like in a standard UV Vis spectrometer. At the same time, the scattered light will reflect insides the cavity to go through the sample several times until it is totally absorbed by the sample (Figure 16).

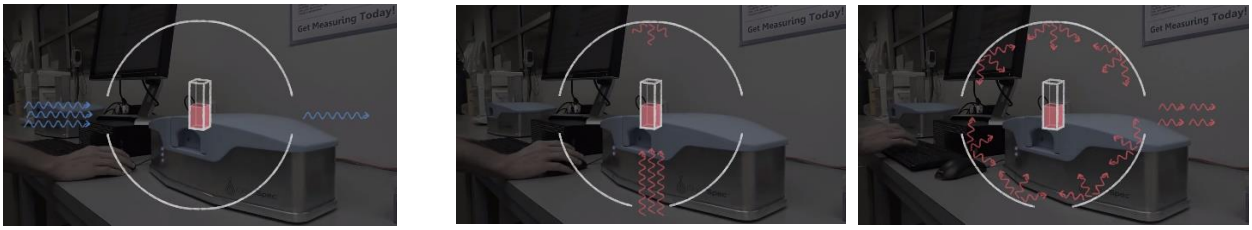

(a) (b)

Figure 16: The measurement process of CloudSpec, (a) extinction measurement, (b) absolute absorption measurement [21].

The measurement of absorption by integrating sphere can provide chemical information of the turbid sample that cannot be processed by a conventional UV Vis spectrometer. The data are automatically calibrated by a proprietary algorithm to provide absorption spectra in 1cm-pathlength equivalent OD, which is illustrated by Figure 17.

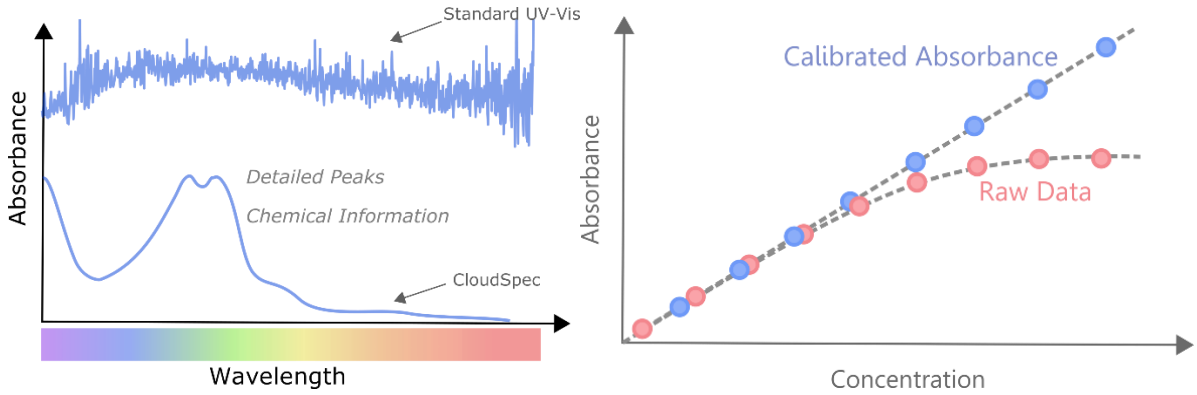

Figure 17: The absorption measurement of CloudSpec [21].

The scattering property of the sample can be computed simply by subtract the data of absorption by those of extinction,

$$\text{Scattering} = \text{Extinction} - \text{Absorption},$$

which means three optical properties of the material can be achieved. Figure 18 illustrates extinction, absorption, and scattering spectra of the sample measured by CloudSpec in one trial.

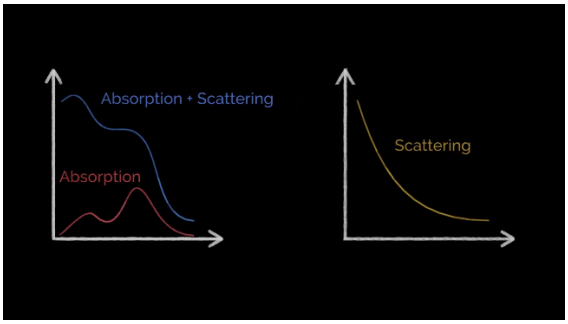

Figure 18: Three optical properties of a turbid sample can be obtained by CloudSpec [21].

Technical specifications: One of the most specific characters of an integrating sphere is its reflectance or its surface's material. The most popular material is Spectralon due to its high reflectivity. In CloudSpec, Fluorilon-99W™ was used. It is a sintered PTFE material with the highest diffuse reflectance, thermal (>300°C), physical, and chemical stability to most of environments. The material has been successfully used in space applications as a calibration target as well as primarily applied as a component in reflective optical systems where the highest diffuse reflectance required [22].

- Reflectance of >99% in the spectral range of 400-800 nm
- Reflectance of >97% in the spectral range of 300-2200 nm
- Reflectance of > 92% in the spectral range of 200-2500 nm

Figures 19 illustrate the reflectance of Fluorilon-99W in UV-Vis-NIR range, i.e. 200-2500 nm, for different wall thickness of the integrating sphere. As can be seen from the graphs, for wall's thickness of 7 mm, the reflectance is reduced significantly in 200-250 nm indicating the light absorption of the sphere in this range. Therefore, the absorption data of the wavelength smaller than 240 or 250 nm are not reliable to consider.

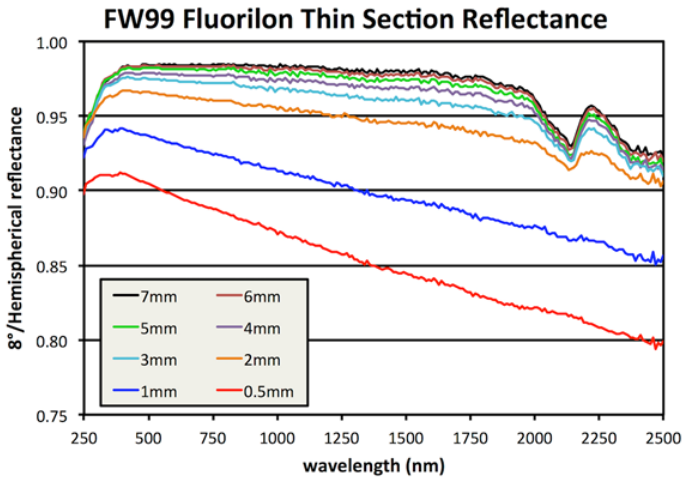
FW99 Fluorilon Thin Section Reflectance
8°/Hemispherical reflectance
wavelength (nm)
7mm
6mm
5mm
4mm
3mm
2mm
1mm
0.5mm

(a)

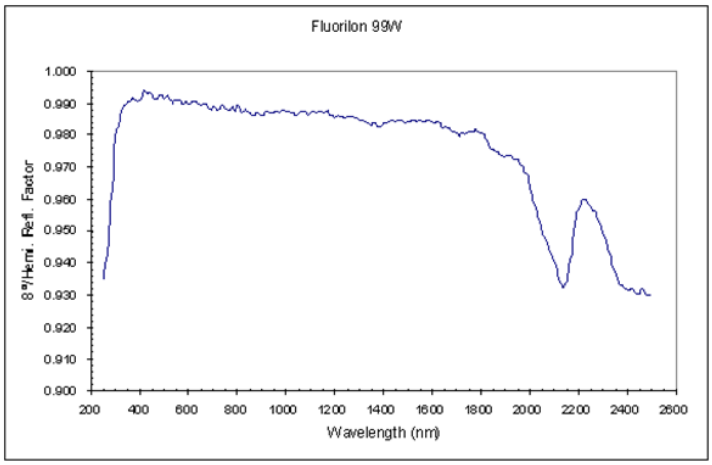
Fluorilon 99W
8°/Hemi. Refl. Factor
Wavelength (nm)

(b)

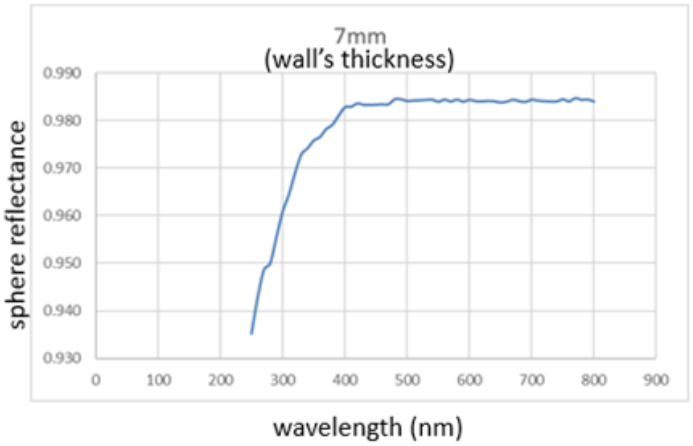
7mm
(wall's thickness)
sphere reflectance
wavelength (nm)

(c)

Figure 19: Reflectance of Fluorilon-99W in 200-2500 nm, (a) for the sphere wall's thickness 0.5-7 mm, (b) and (c) for the wall thickness of 7 mm [22].

Figure 20 give information about main parameters of CloudSpec. It is noticeable that CloudSpec can perform standard UV Vis spectroscopy, i.e. extinction spectroscopy, in the wavelength range of 200-800 nm and diffuse-light absorption spectroscopy or absolute absorption in the wavelength range of 240-800 nm. The data of the lower wavelength than 240 nm are not reliable for the absorption spectroscopy because the sphere surface also absorb light in those spectra. In addition, absorbance range is from 0.005A-1A for 10 mm path length cuvette and 0.05A-10A for 1 mm path length cuvette. The instrument can measure samples with high turbidity, i.e. 4000 NTU. The resolution of the spectra is 3 nm. And the measurement time is quite fast, around 10 seconds for a trial.

Parameter	CloudSpec-UV
Instrument Type	Single-beam
Dectector Type	2048 Pixel CCD
Light Sources	Pulsed Xenon
Wavelength Range	250nm-800nm
Measurement Modes	Absorption and Transmission
Cuvette Types	Suprasil Quartz (1mm, 10mm)
Absorbance Range	0.005 A – 1A (10mm) 0.05 A – 10A (1mm)
Turbidity Range	4000 NTU
Resolution	3nm
Measurement Time (approx.)*	Total Phenolics: 10 seconds Colour: 4-5 seconds
Footprint	45cm (W), 30cm (D), 15cm (H)

*Not including sample preparation time (i.e. dilution steps)

Figure 20: Technical specifications of CloudSpec [21]

Applications: For a non-scattering sample such as clear dye solution, the two spectra – extinction and absorption are the same. The ICAM technique is therefore useful for a broad range of scattering samples like suspension and emulsion. For example, CloudSpec was used to measure absorption, extinction, and scattering spectra of metallic nanoparticles, i.e. silver and gold nanoparticles [23]–[25]. It was shown that in comparison with the extinction spectrum, the absorption spectrum was significantly more sensitive to subtle shape effects (such as surface roughness). It was also considered that in addition to the extinction spectra, the additional absorption spectrum allowed more accurate nanoparticle-size determination. Furthermore, recent work shows that CloudSpec is promising in bacterial characterization [26]. Because the instrument has only been recently commercialized, several possible other applications, particularly in winery, beverage, and pharmaceutical industries, are shown on Marama Labs website with no publication available [21].

RESEARCH

The research aims to apply the combined extinction/absorption spectroscopy of CloudSpec to investigate the optical properties of the materials – extinction, absorption and scattering, and to extract chemical information of turbid or strongly scattering samples through the absolute absorbance that could not be studied by a standard UV Vis spectrometer. The method is promising for practical samples in environment, food, and biomedicine. Three projects were under progress – dairy analysis, microplastics study, and vitamin assessment (i.e. the dissolution study).

CHAPTER 2 – DAIRY ANALYSIS

2.1. Literature review

Dairy products are important sources of daily nutrition such as carbohydrate, lipid, protein, vitamins, and minerals [27].

MilkoScan and LactoScan are typically commercial instrument to estimate quality of dairy products [28]. The MilkoScan is based on Fourier Transform Infrared measurements (FT-IR) with spectral range of 2,500-25,000 nm while the LactoScan is based on the ultrasonic technique. Although they are commonly-used techniques, both systems are offline as they require the transportation of the products to the laboratory where the instrument is installed. Whereas, daily monitoring of milk composition on farm plays a crucial role in milk quality because it helps farmers adjust their farming on time.

Many new techniques have been developed during the last decades to determine nutrients in milk with the objectives of cost-efficiency, online, and non-invasiveness. They are based on the principles of nuclear magnetic resonance (NMR), conventional digital imaging, ultraviolet illumination, visible light effects, infrared spectroscopy, electrical conductivity, fiber-optic sensors, etc. [28].

Recently, the low-cost MicroNIR spectrometers are developed [29]. The infrared spectrometers include MicroNIR1700 for analyzing the 870-1660 nm region and MicroNIR2200 for analyzing the 1130-2150 nm region. Although they needed modified, they were promising for examining raw milk on-farm. According to the data, MicroNIR1700 could predict fat and protein with root mean square errors (RMSEs) of 0.061 and 0.151 respectively. Whereas, MicroNIR2200 could do that with RMSEs of 0.061 and 0.138. Their modified versions, which had the enhancement for signal-to-noise ratios and the cooling systems for the increase of the temperature, could meet the requirements for fat and protein precision limits of the International Committee for Animal Recording (ICAR).

Another recent work in this field is the application of the integrating sphere and Mie theory for determining the concentration of main scattering components in milk, i.e. fat globules and casein micelles based on their scattering properties [30]. The system consisted of the integrating sphere setup with two spectrometers in 180-1100 nm and in 900-1700 nm. Size measurements were conducted to investigate the impact of fat globule size on the scattering properties. In addition, Mie theory calculations were applied on scattering spectra to examine the correlation among the concentration of fat, protein, their particle sizes, and their scattering properties. Some of the positive correlations were found but need further research.

Main nutrition components in milk are fat (3.7%), protein (3.4%), and lactose (4.8%) [27]. Besides, there are minerals, particularly calcium, and a variety of organic substances such as beta-carotene, riboflavin, and hemoglobin (in raw milk) [30].

Milk fat is made of three groups of fatty acids – saturated (65%), monounsaturated (30%), and polyunsaturated (5%) [27]. The fatty acids are arranged on the triglyceride molecule with a particular shape which affects the properties of milk fat. The triglycerides are in form of globules, surrounded by a protein and phospholipid membrane which make their stability in serum phase of milk. The globule size range is approximately 1-10 µm. Milk is homogenized to reduce the globule size to below 1 µm while cream contains large globules [27]. Milk fat absorbs UV radiation at the three wavelengths of 205 nm, 230 nm, and 270 nm. The absorption at 205 nm results from the presence of double bonds in the fatty acyl

groups while the absorption at 230 nm and 270 nm come from the conjugated dienes and trienes of UFA [31].

Milk protein has two types – casein and whey. The casein is suspended in milk in a spherical shape called micelles with the diameter range of 0.04-0.3 µm. The high phosphate content of casein forms with calcium to make calcium phosphate salts and provide a good source of calcium. Whereas, the whey protein does not contain phosphate but a large amount of sulfur amino acids, forming disulfide bonds within the protein and making a spherical shape [27]. Most proteins strongly absorb UV radiation at the wavelength of 280 nm due to their tryptophan content [32].

Milk carbohydrate is predominately lactose (a disaccharide of glucose and galactose). Lactose is dissolved in the serum phase of milk [27].

Main scattering components in milk are fat globules (emulsion), and casein micelle (dispersion). Whereas, whey protein and lactose form solution. Figure below shows the distribution of fat globules and casein micelles in milk under the microscopic view.

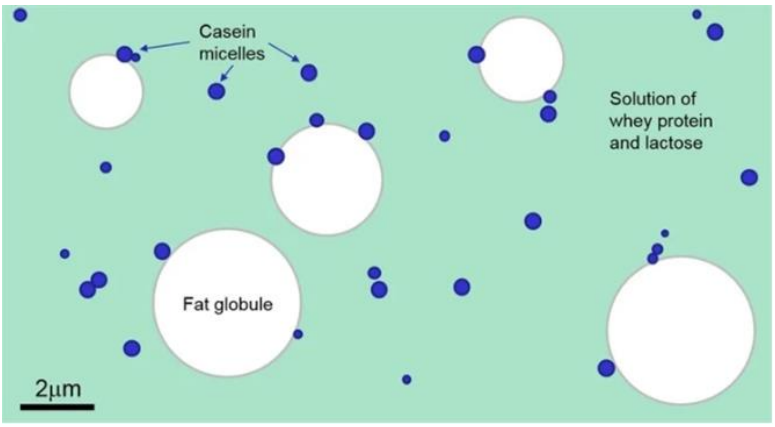

Figure 21: Fat globules and casein micelles in milk [33].

Dairy components and their corresponding UV-Vis absorbance maxima are presented in Table 1.

Nutrient	Component	Shape	Diameter	Absorption
Fat (3.7%) [28], [30], [31], [34]	Triglyceride (65% saturated fatty acids, 30% monounsaturated, 5% polyunsaturated) Phospholipid	globules	< 1 µm (milk) 1-10 µm (cream)	205 nm (double bond in fatty acyl group), 230 nm and 270 nm (conjugated dienes and trienes of UFA), 460-470 nm, > 600 nm, > 700 nm
Protein (3.4%) [18], [28], [32], [35]	casein (82%)	micelles	0.04-0.3 µm	290 nm, 217 nm
	whey (18%)	spherical		294 nm, 283 nm, 214 nm
				280 nm (tryptophan content)

Lactose (4.8%) [Sigma Aldrich]	disaccharite (glucose+galactose)	dissolved in serum (whey) phase of fluid milk		400 nm, 210-220 nm, 270-300 nm
Retinol [28], [36]		fat-soluble		328.5 nm
Beta-caroten [28], [30], [36]				440 nm, 460 nm
Riboflavin [28], [30], [37]		water-soluble		370 nm, 440 nm, 470 nm
Calcium [38]		forms phosphate salts with casein	nanoclusters	275-276 nm

Table 1: Dairy components and corresponding UV-Vis absorbance maxima.

2.2. Project description

The research aimed to qualify and quantify major nutrition components such as fat and protein in dairy products, specifically milk and cream, using CloudSpec instrument (Marama Labs), which implements a newly developed UV Vis Spectroscopy technique, i.e. Combined Absorption/Extinction Spectroscopy. In the case of milk/cream, the extinction spectra are completely saturated because of strong scattering, but an absorption spectrum (which is scattering independent) can be obtained.

2.3. Qualitative analysis

Experiments: Dairy products of two commercial brands were analyzed, symbolized brand A and brand F.

Nutrient information of the three dairy product types of brand A is shown in Table 2.

Nutrient	Whole milk	Skim milk	Cream
Protein	3.3g	4.0g	2.4g
Fat	3.4g	0.1g	37.3g
Carbohydrate	4.8g	5.0g	3.0g
Sodium	40mg	41mg	25mg
Calcium	117mg	133mg	0
Vitamin A	45µg	0	0
Riboflavin (B_2)	0.2mg	0.2mg	0

Table 2: Nutrition information in 100ml of brand A's products - whole milk, skim milk, and cream.

As can be seen from the figure above, there are large discrepancies of fat content in the three dairy types. Particularly, Whole Milk contained more than 30 times the fat than Skim Milk and Cream was a further 10 times higher in fat than Whole Milk. In addition, the concentration of protein also differed in Whole Milk, Skim Milk, and Cream. Another thing to note is that there were mineral and vitamins in Whole Milk and Skim Milk, i.e. Calcium, Vitamin A, and Riboflavin, which Cream did not include.

Information of 13 products of brand F is shown in Table 3.

Product Streams	Fat (% m/m)	Protein (% m/m)	Lactose (% m/m)	Total Solids (% m/m)
Filtered Milk	4.88	3.71	4.67	14.09
	4.88	3.69	4.67	14.10
Butter milk	0.86	3.39		9.52
	0.85	3.40		9.55
Cream	43.54	2.15		49.22
	43.28	2.16		48.98
Skim milk	0.04	3.90	4.88	9.75
	0.05	3.87	4.87	9.77
Permeate 6%		0.22		5.53
		0.22		5.54
Permeate 12%		0.42		12.33
		0.43		12.33
RO milk	8.49	6.36		24.47
	8.50	6.37		24.49
Cheese whey	0.03	0.97		6.10
	0.03	0.97		6.12
Lactic whey	0.02	0.79		5.03
	0.03	0.80		5.04
Retentate	0.12	10.89	4.22	16.86
	0.13	10.92	4.22	16.82
Standardized Streams				
P 5	3.56	3.16	5.15	12.71
	3.57	3.18	5.17	12.73
CH 2	3.27	4.32	4.23	12.71
	3.27	4.33	4.27	12.69
CH 1	5.27	4.33	4.58	15.06
	5.27	4.33	4.56	15.11

Table 3: Nutrition information of brand F's products.

The samples were measured directly by the instrument without dilution or treated. Only 1ml of each product needed to be used for the measurement.

Results: As expected, there was no information from the extinction spectra due to the turbidity of the samples so all data shown below correspond to the absorption spectra.

Figures 22 show the absorption spectra of brand A's samples, i.e. whole milk, trim milk, and cream.

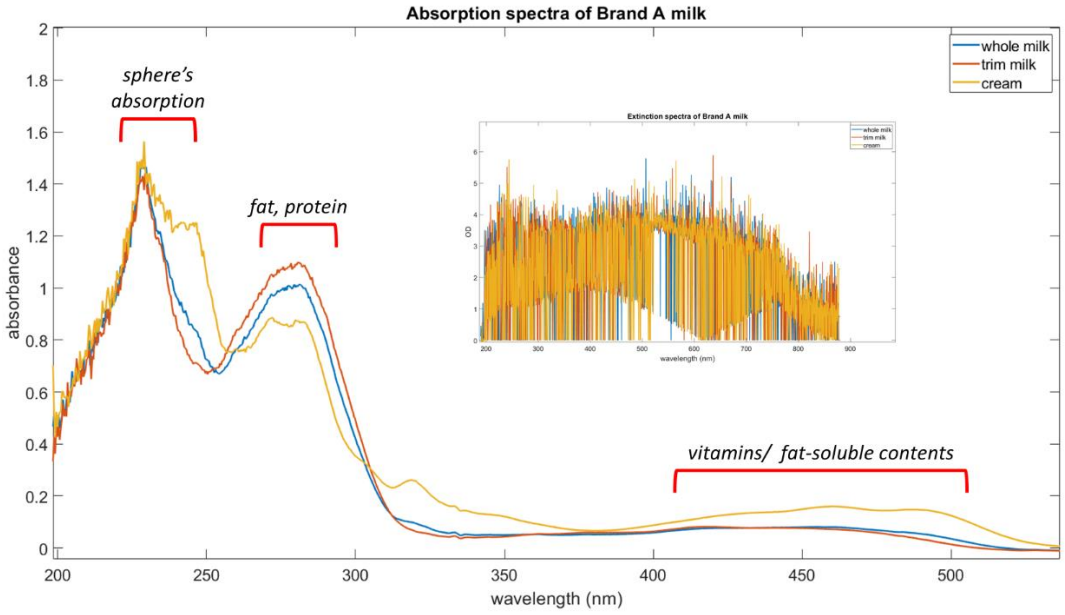
Absorption spectra of Brand A milk
whole milk
trim milk
cream
sphere's absorption
fat, protein
vitamins/ fat-soluble contents
absorbance
wavelength (nm)
Extinction spectra of Brand A milk

(a)

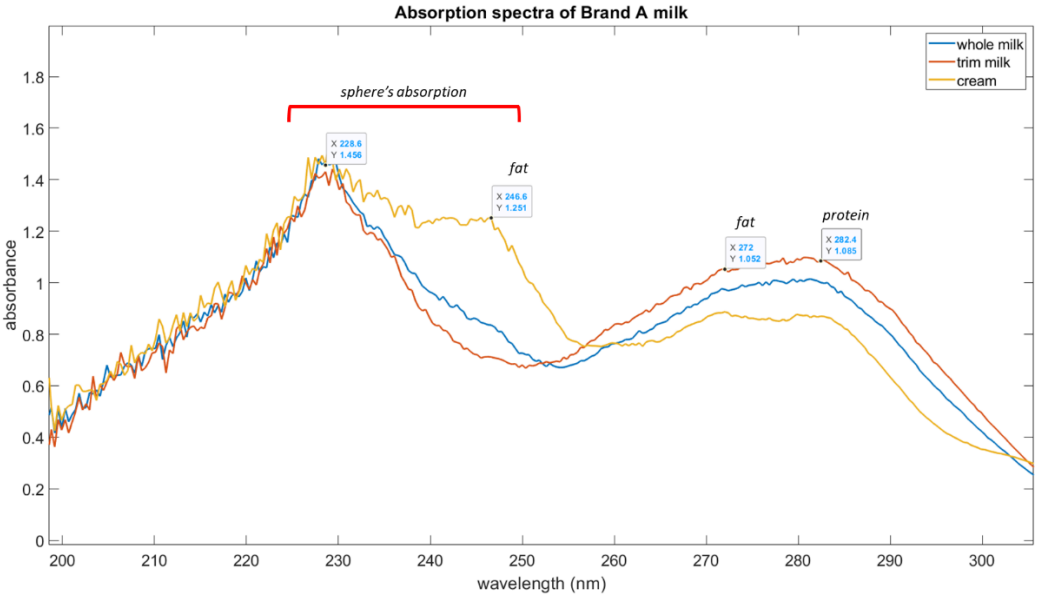
Absorption spectra of Brand A milk
whole milk
trim milk
cream
sphere's absorption
X 228.6
Y 1.456
fat
X 246.6
Y 1.251
fat
X 272
Y 1.052
protein
X 282.4
Y 1.085
absorbance
wavelength (nm)

(b)

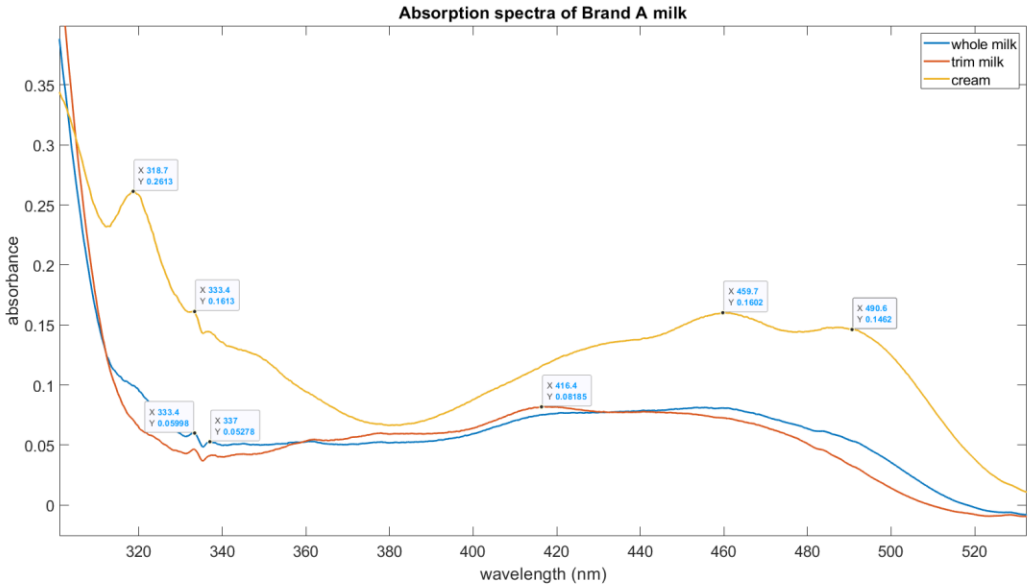

(c)

Figure 22: Absorption spectra of brand A's products, (a) in 200-800 nm range, (b) in ultraviolet range, and (c) in visible range.

As can be seen from the graphs (Figure 22), the extinction spectra were totally saturated so we could not examine them. Whereas, the absorption spectra were clear and provide useful information about the samples, i.e. whole milk, trim milk, and cream. The peak at 228 nm was due to the sphere's absorption because in 200-240 nm the sphere cavity surface also absorbed light.

It is noticeable from graph in UV range that there were two peaks at 246 nm and 272 nm considered as the maxima absorbance of fat components and the peak at 282 nm considered as the maxima absorbance of protein components. We note that calcium also absorbs around 275 nm so may not be distinguished from fat. The peaks in 320-340 nm are attributed to vitamin A (see Table 1) which is oil-soluble. In visible-range graph, we can observe there was a number of peaks, which can be attributed to beta-carotene (440 nm, 460 nm), a common component in milk and cream. Note that vitamin B2, which is water-soluble, also absorbs in this region (370 nm, 440 nm, 470 nm).

Figure 23 represent the absorption spectra of brand F's products.

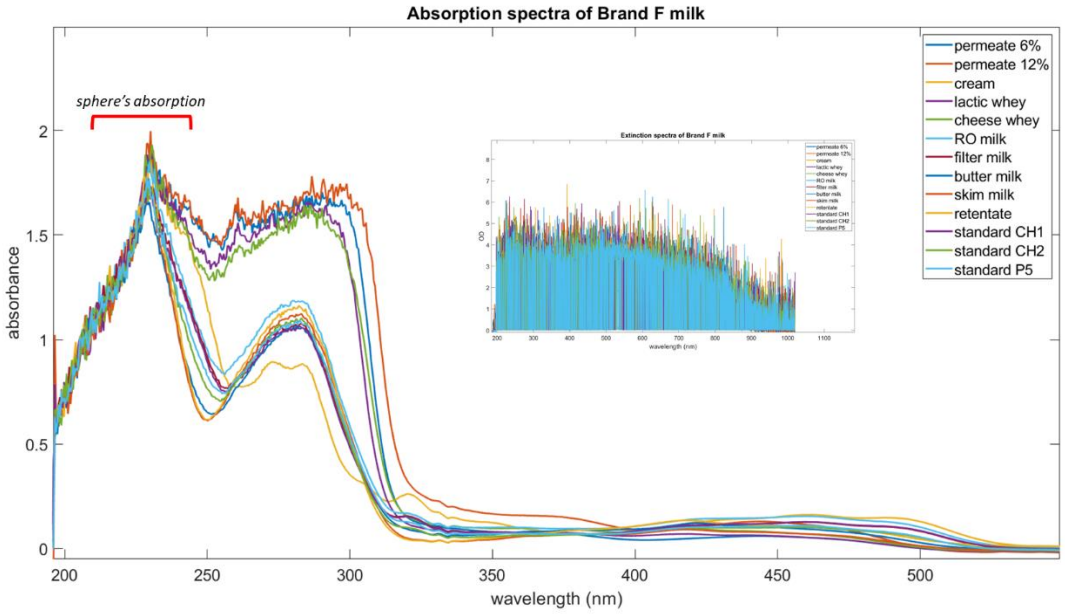
Absorption spectra of Brand F milk
sphere's absorption
absorbance
wavelength (nm)
permeate 6%
permeate 12%
cream
lactic whey
cheese whey
RO milk
filter milk
butter milk
skim milk
retentate
standard CH1
standard CH2
standard P5

(a)

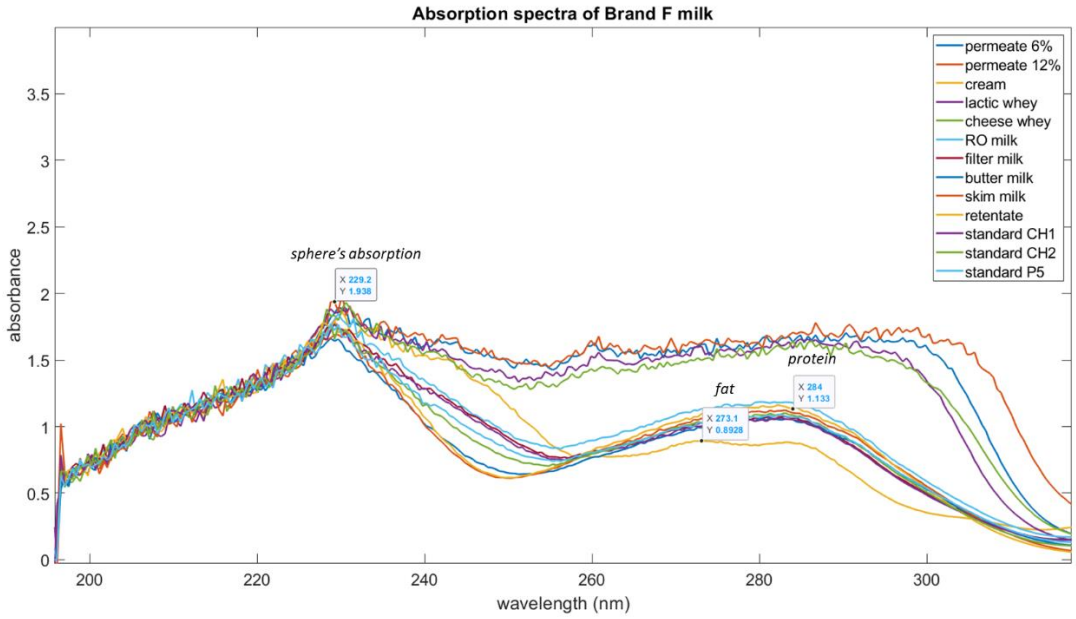
Absorption spectra of Brand F milk
sphere's absorption
X 229.2
Y 1.938
protein
fat
X 284
Y 1.133
X 273.1
Y 0.8928
absorbance
wavelength (nm)
permeate 6%
permeate 12%
cream
lactic whey
cheese whey
RO milk
filter milk
butter milk
skim milk
retentate
standard CH1
standard CH2
standard P5

(b)

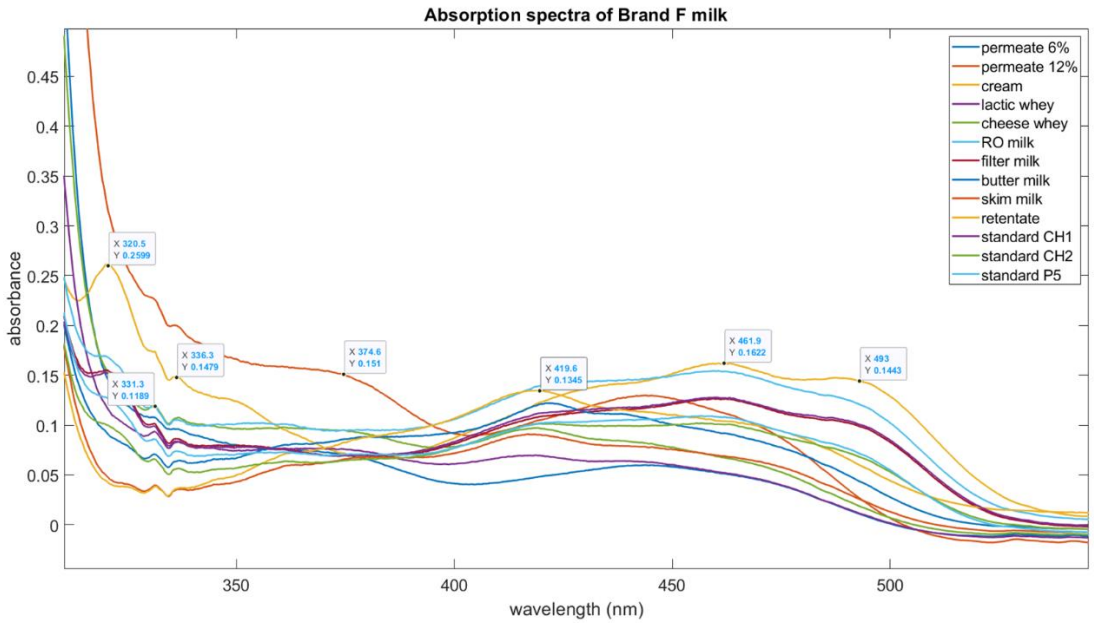

(c)

Figure 23: Absorption spectra of brand F's products, (a) in 200-800 nm range, (b) in ultraviolet range, and (c) in visible range.

As can be seen from the graphs (Figure 23), the extinction spectra were saturated completely and peak at the wavelength lower than 240 nm was the sphere's absorption. In UV-range graph, we can see the peak of fat at 273 nm and the peak of protein at 284 nm. Whereas, in visible-range graph, there was a number of peaks in the wavelengths of 320-380 nm, 459 nm, and 490 nm but we could not conclude anything here because the provided nutrition information did not mention any vitamin in brand's F products.

Discussions:

There are similar peaks in products of both brands – 270 nm which can be triglyceride fat, 280 nm of protein due to the tryptophan content, 283 nm and 294 nm of whey protein. The shift of peaks in 3 nm is considered to come from the resolution of the instrument. Also, peaks at wavelength less than 240 nm are not reliable due to the cavity absorption.

Peaks of vitamin A – 328 nm and vitamin B2/beta-carotene – 440 nm, 460 nm, 470 nm are thought to appear in spectra of brand A products.

2.4. Quantitative analysis

Brand A: To quantify major nutrients in dairy product, whole milk and skim milk were mixed together with different percentages of volume to create Milk Blends. Similarly, cream was diluted with skim milk to create a range of Cream Blend. Table 4 describes how the sample were made as well as their percentage of fat - %Fat (g/ml), protein concentration – $C_{Protein}$ (mg/ml).

Blended Milk Samples

$\%V_{Blue\ Milk}$	0%	20%	40%	60%	80%	100%

%V Trim Milk	100%	80%	60%	40%	20%	0%
Samples	W0	W20	W40	W60	W80	W100
%Fat (g/ml)	0.1%	0.68%	1.36%	2.04%	2.72%	3.4%
C Protein (mg/ml)	40	38.6	37.2	35.8	34.4	33

Blended Cream Samples

Dilution	2^0	2^1	2^2	2^3	2^4	2^5
	1	2	4	8	16	32
Samples	Cr	CrDil2	CrDil4	CrDil8	CrDil16	CrDil32
%Fat (g/ml)	37.30%	18.65%	9.33%	4.66%	2.33%	1.17%
C Protein (mg/ml)	24	32	36	38	39	39.5

Table 4: Sample preparation for Milk Blends and Cream Blends.

Water was taken as reference then Milk Blends and Cream Blends were measured. Calibrated ODs of absorption and extinction were computed automatically by the instrument software. Raw intensity data are also available, which allows us to compute measured absorbance (non-calibrated) but this was not used here.

All the spectra are broadly similar, so in order to highlight the changes, we subtracted to every spectrum to the trim milk spectrum. Figure 24 shows absorption spectra of milk blends and cream blends relative to trim milk.

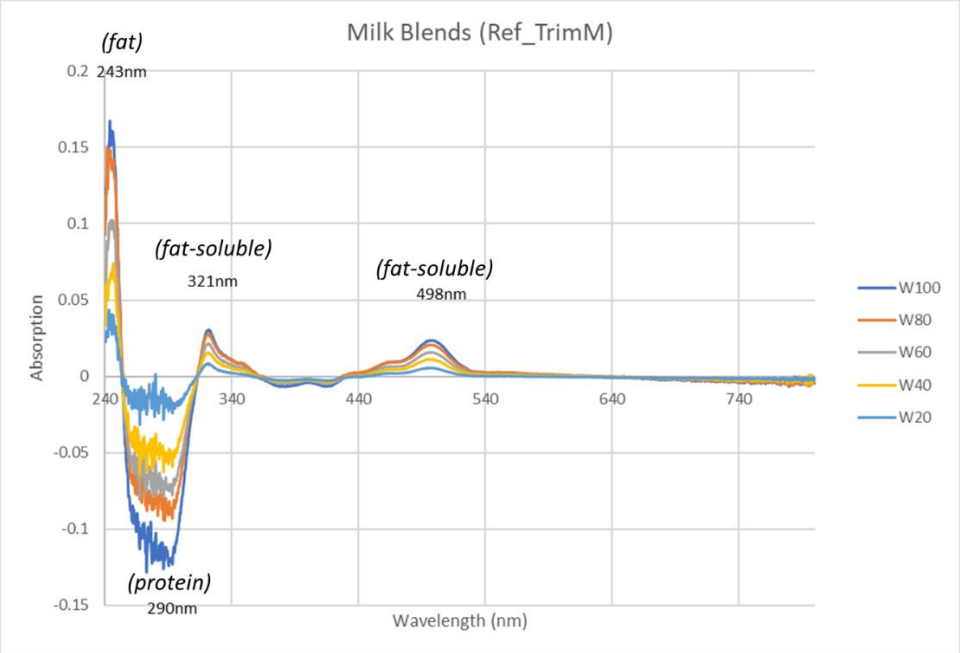

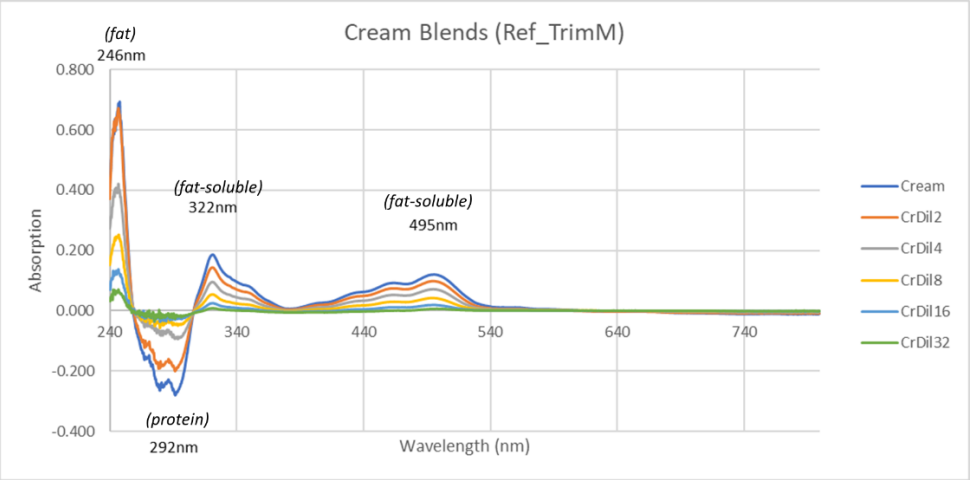

Figure 24: UV-vis absorption spectra (240-800 nm) of milk blends and cream blends taking trim milk as reference.

As can be seen from the graphs (Figure 24), there were three major ranges of peak, i.e. around 243-246 nm, 321-322 nm, and 495-498 nm, having positive correlation with the percentage of fat. These are tentatively attributed to fat content. Another range of peak around 290-292 nm has negative correlation with fat content but positive relation with protein concentration and is therefore attributed to protein content.

The absorption OD dependence on fat content was plotted at four wavelengths of interest – 243 nm, 321 nm, 498 nm, and 450 nm as shown below. The dependences are linear, but note that they do not go through zero, as one would expect from Beer Lambert law if these peaks were fat only.

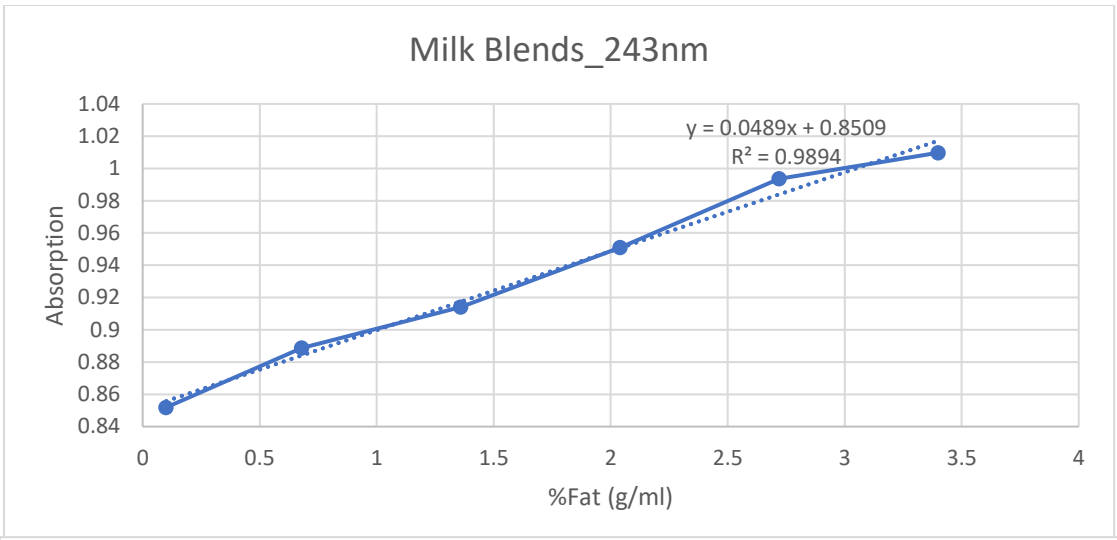
Milk Blends_243nm
y = 0.0489x + 0.8509
R² = 0.9894
Absorption
%Fat (g/ml)

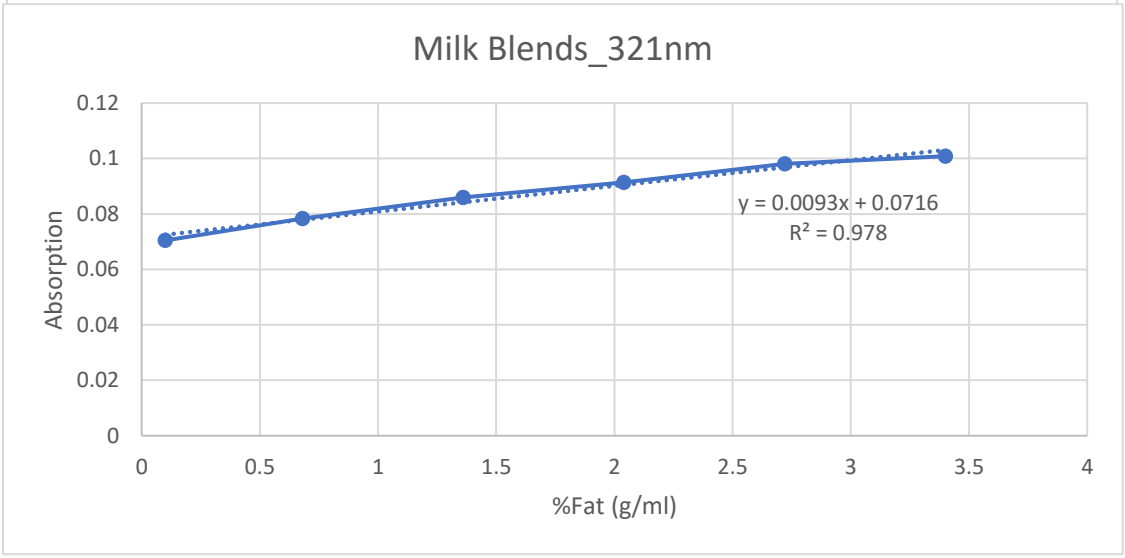
Milk Blends_321nm
y = 0.0093x + 0.0716
R² = 0.978
Absorption
%Fat (g/ml)

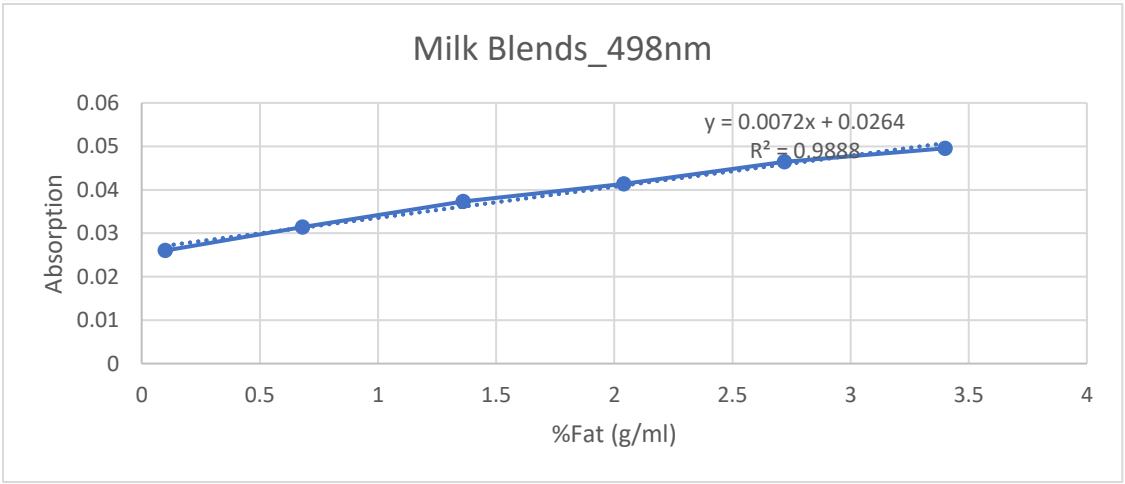
Milk Blends_498nm
y = 0.0072x + 0.0264
R² = 0.9888
Absorption
%Fat (g/ml)

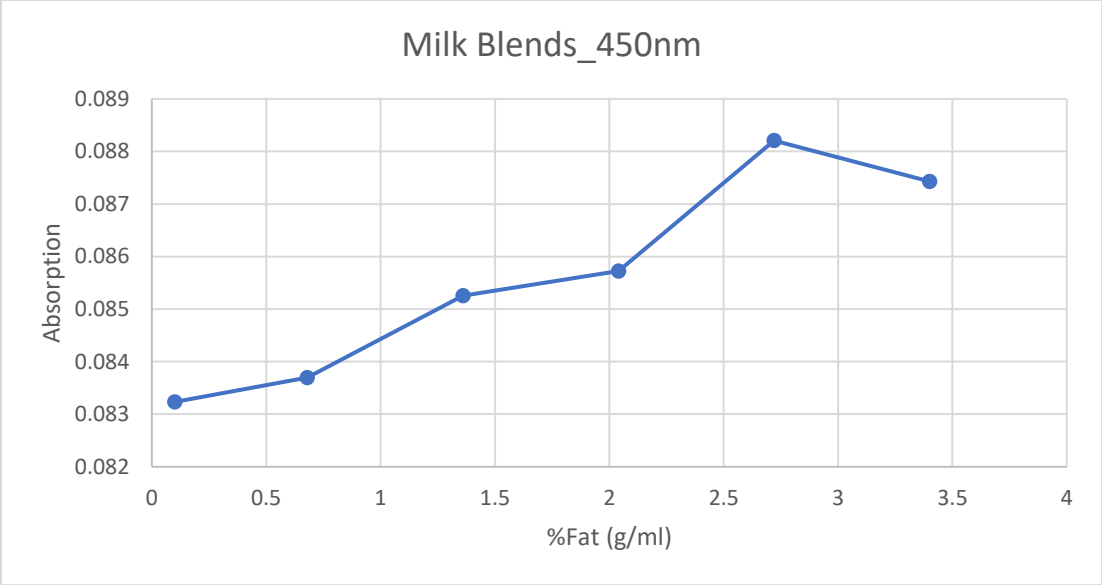

Figure 25: Fat dependence of milk blends absolute absorbance at four peaks – 243 nm, 321 nm, 498 nm and 450 nm.

Similar graphs (Figure 26) are shown below for the relative absorbance (compared to Trim milk).

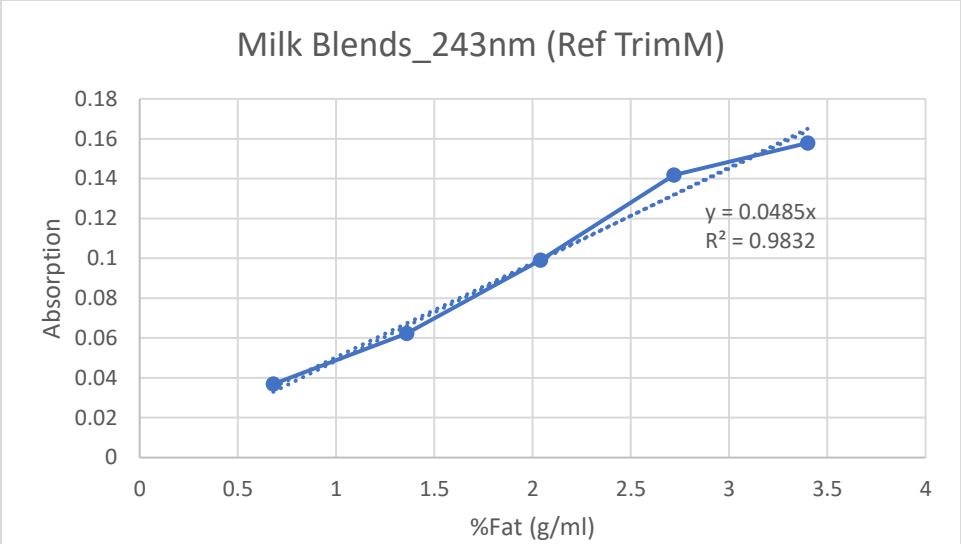
Milk Blends_243nm (Ref TrimM)
Absorption
0.18
0.16
0.14
0.12
0.1
0.08
0.06
0.04
0.02
0
0
0.5
1
1.5
2
2.5
3
3.5
4
%Fat (g/ml)
y = 0.0485x
R² = 0.9832


Milk Blends_321nm (Ref TrimM)
Absorption
0.035
0.03
0.025
0.02
0.015
0.01
0.005
0
0
0.5
1
1.5
2
2.5
3
3.5
4
%Fat (g/ml)
y = 0.0097x
R² = 0.9502

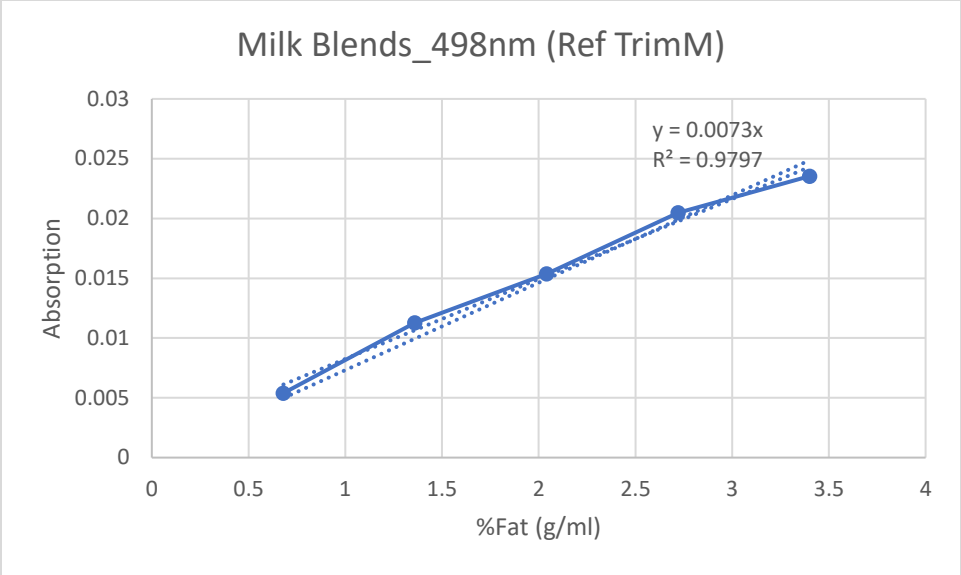

Figure 26: Fat dependence of milk blends absorbance relative to trim milk at four peaks – 243 nm, 321 nm, 498 nm and 450 nm.

Graphs for absolute OD of cream are shown below (Figure 27). The dependence is no longer linear. The milk results are also included for comparison. Note that the absorbance at 243 nm is too high to be reliable.

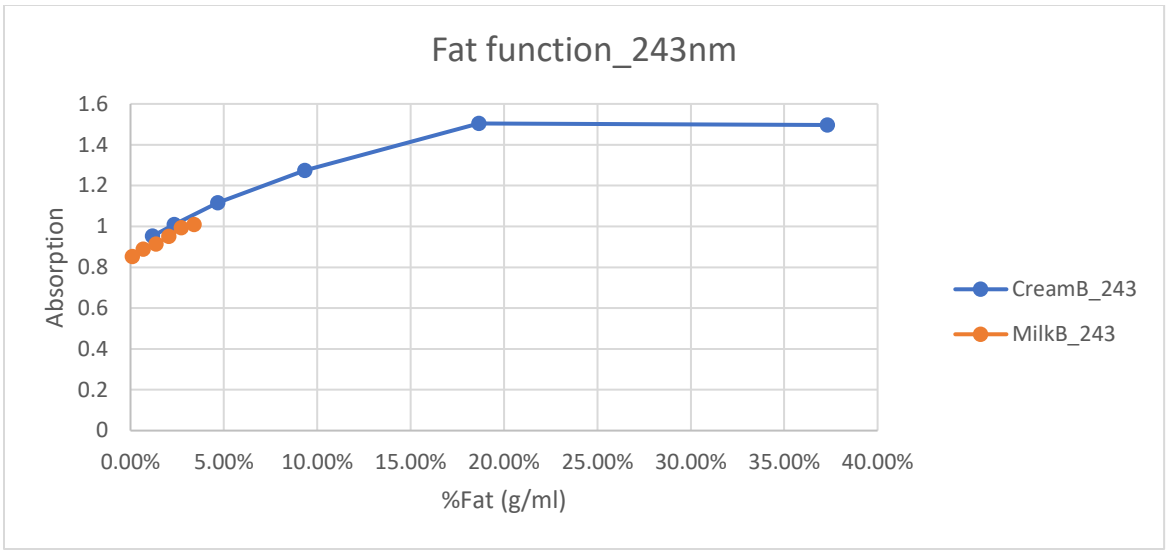
Fat function_243nm
Absorption
1.6
1.4
1.2
1
0.8
0.6
0.4
0.2
0
0.00%
5.00%
10.00%
15.00%
20.00%
25.00%
30.00%
35.00%
40.00%
%Fat (g/ml)
CreamB_243
MilkB_243

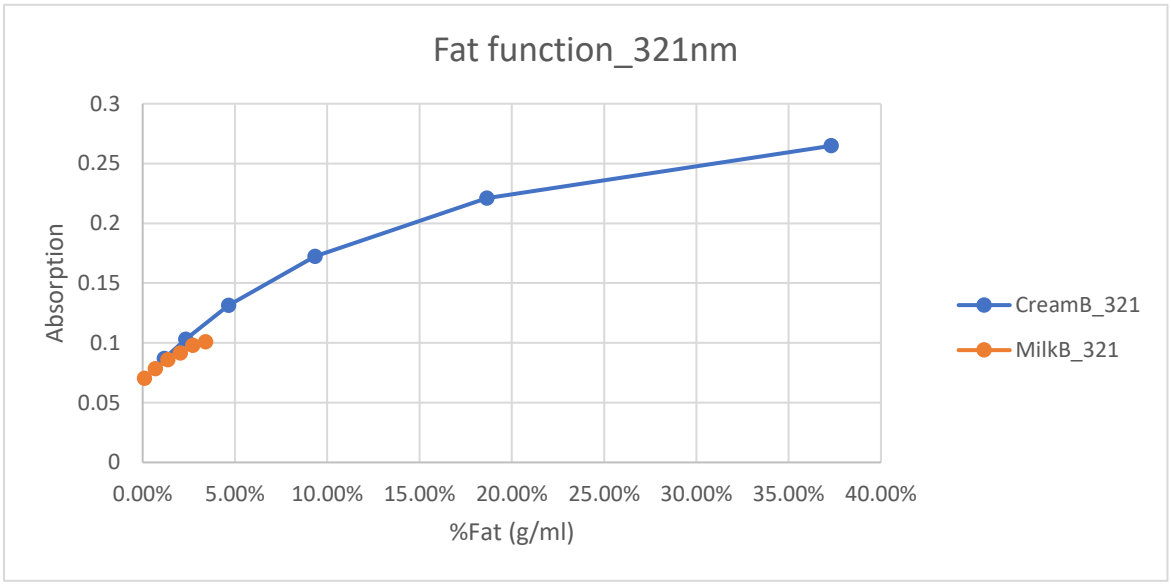
Fat function_321nm
Absorption
0.3
0.25
0.2
0.15
0.1
0.05
0
0.00%
5.00%
10.00%
15.00%
20.00%
25.00%
30.00%
35.00%
40.00%
%Fat (g/ml)
CreamB_321
MilkB_321

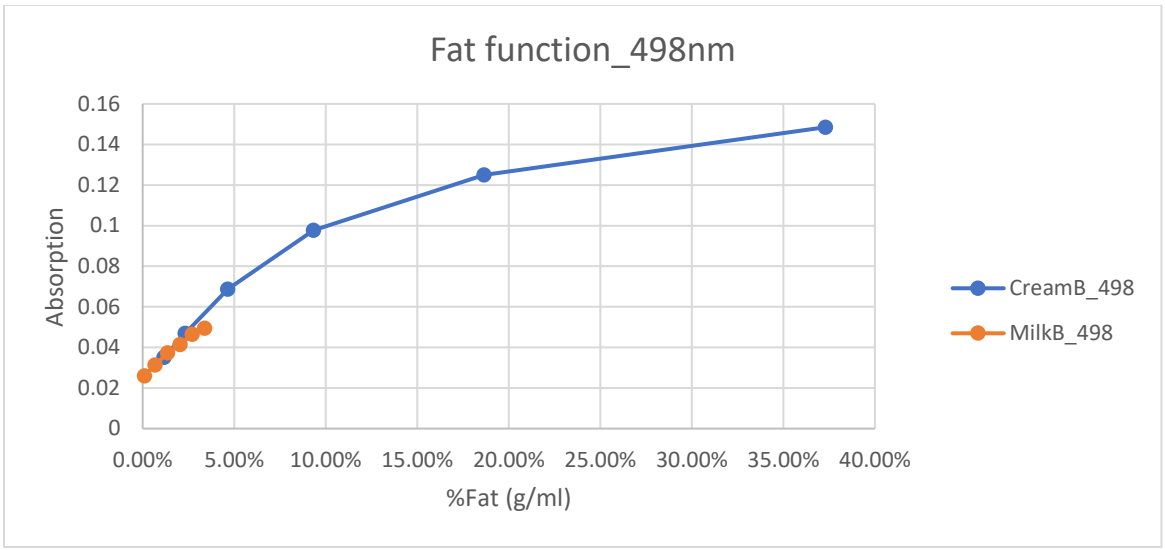

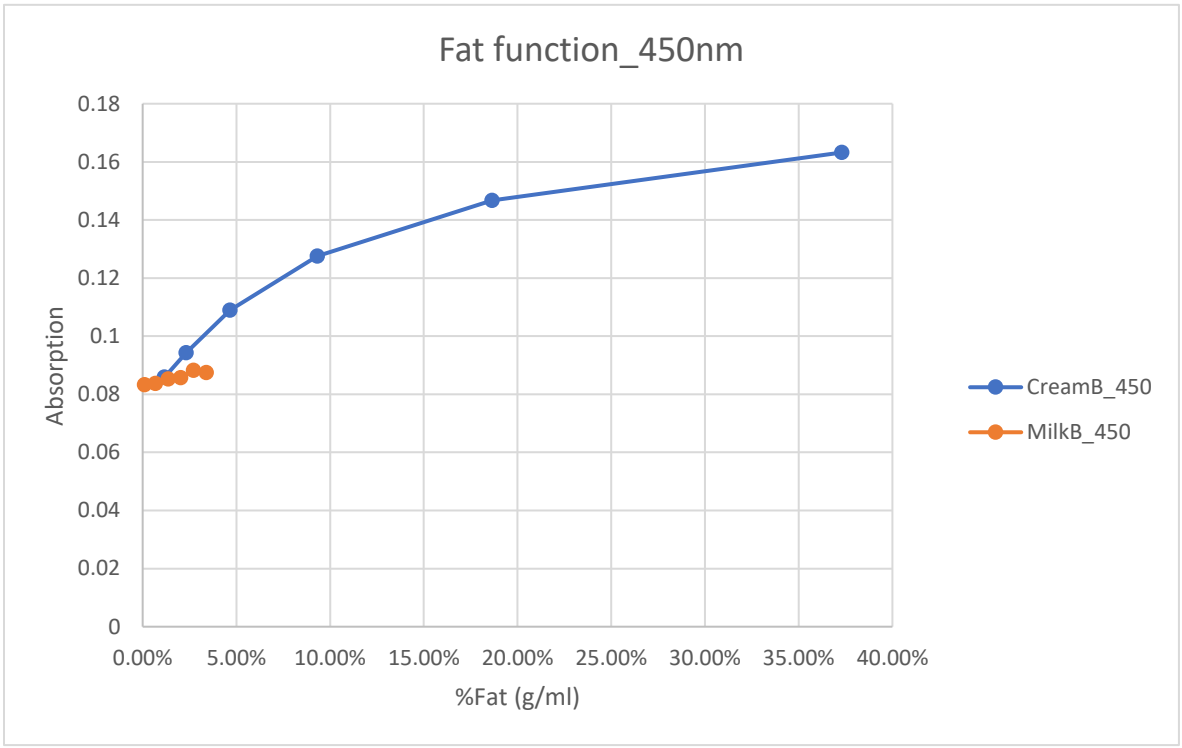

Figure 27: Fat dependence of cream blends absolute absorbance at four peaks – 243 nm, 321 nm, 498 nm, and 450 nm.

Similarly, the dependence on protein content was studied for the absorbance at wavelength 290nm for milk and cream blends as summarized below (Figure 28).

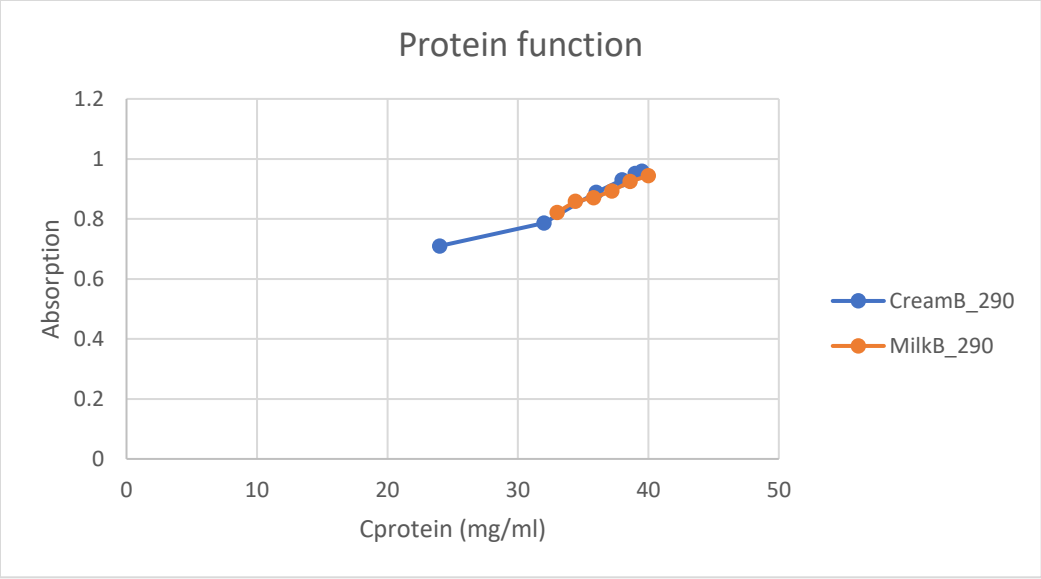

Figure 28: Protein function of milk blends and cream blends taking water as reference at wavelength 290 nm.

We can clearly see trends as a function of fat content. The peaks at 321 nm and 498 nm for example can be used to measure fat content in binary mixtures of skim and whole milk like shown here.

However, there seems to be other contribution to the absorbance at 322 nm and 498 nm, as they are far from being zero in trim milk. The variability of these contributions from sample to sample could significantly affect our ability to quantify fat content. There is some (small) evidence of this when comparing the milk blend and cream blend results. Further tests would need to be done on samples representative of the expected variability.

The strong non-linearity of the cream absorption also suggests that complicating mechanisms are at play. One of these could be the micellar nature of milk. If the micelles are too big, then light could be absorbed on their surface and any component closer to the center of the micelle would be invisible. If the micellar structure is dependent on fat content, then it could affect our measurements. This may explain the non-linear cream results and would also require further investigation.

Similar conclusions and comments can be drawn regarding the protein content, with a characteristic absorbance peak at 280 nm. It should be noted however that the absorbance there is quite close to saturation so results are less reliable. Dilutions might be needed (or some adaptation of the instrument) to make protein measurements more accurate.

Finally, we have not tried to consider the possible effect of vitamin A or riboflavin, which likely contribute to the peaks around 400 nm.

2.5. Discussion, conclusion and outlook

To conclude, peaks of fat, protein, vitamin A, vitamin B2, and beta-carotene were observed in absorption spectra of two commercial dairy brands. The samples included a variety of milk types as well as cream and

cheese with different percentages of those nutrients. Functions of fat and protein content in the prepared samples displayed a positive linearity in the low concentration.

Some aspects will require further studies – for example, the shift of peaks, spectrum overlap, and the non-linearity of the function of fat and protein content in high concentration.

For the shift of peaks, impact factors such as chemical structure of the substances and pH of the media should be considered when comparing the experimental data with the reference's data. Study of the resolution (3 nm) of the instrument (CloudSpec) should be conducted.

For spectrum overlap, multiple component analysis could be considered. This is beyond the scope of the present work, but we hope to use the current comprehensive dataset for further statistical analysis with methods such as Partial Least Square, which could potentially reveal non-obvious correlations between the measured spectra and the milk composition, for example fat content.

Finally, for the non-linearity, the formation of fat globules and casein micelles or their size ranges in a variety of dairy samples, which increase the amplitude of the absorbance maxima and disobey the Beer's law, should be investigated.

CHAPTER 3 – MICROPLASTICS STUDY

3.1. Introduction and literature review

Microplastics: Microplastics, waste from domestic plastics, have recently existed in the air and been reported to affect the global climate [39]–[44]. Directly, if they absorbed the sunlight, the atmosphere will be heated locally but cool at the surface. In contrast, if they scatter the sunlight, less sunlight will reach the earth leading to the cooling. The interactions depend on their size, shape, and composition. Indirectly, airborne microplastics also take part in cloud formation, atmospheric circulation, and rainfall patterns. The direct and indirect impacts of microplastic aerosols on climate are illustrated by Figures 29, 30.

p

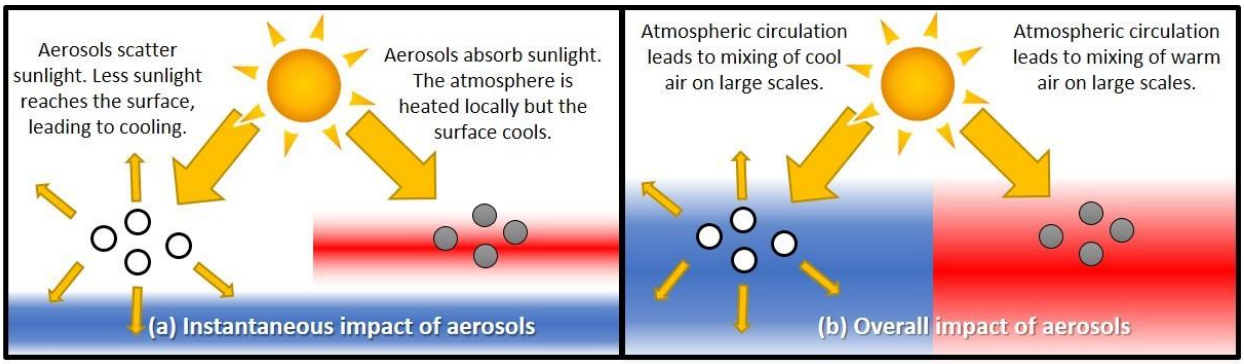

Figure 29: Theoretically instant impact and long-term impact of microplastics in the air [45].

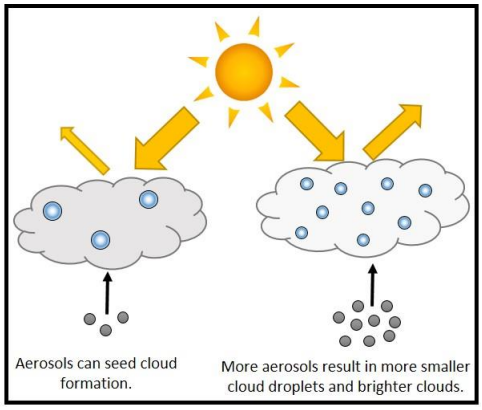

Figure 30: Simplified overview of aerosol-cloud interactions [45].

For investigating their impacts on global scale, three steps will be conducted. The first is to collect atmospheric microplastics in reported areas. The second is to extract their optical properties, i.e. absorption and scattering. Finally, the data – size distributions and atmospheric abundances (step 1) and the measured optical properties (step 2) will be implemented into a chemistry-climate models consisting of a dynamical core which simulates pressure, temperature and winds, interactively coupled to atmospheric chemistry, aerosol, radiation and cloud microplastics schemes [46]. However, it a multi-disciplinary collaborating projects in which the work of this thesis will contribute to step 2 – extracting optical properties of the microplastics using a spectroscopic method optimized for nanoparticles, supported by electromagnetic calculations.

The complex refractive index (CRI) of plastics is needed to predict the optical properties (i.e. absorption and scattering) of microplastics fragment in the atmosphere. The CRI is defined by two components – the real part and the imaginary part which represent for refractivity/scattering and absorption coefficient/ absolute absorption of the material, respectively:

$$n = n_0 + ik$$

, where n is the complex refractive index, n_0 is the real part or refractive index, k is the imaginary part or absorption coefficient.

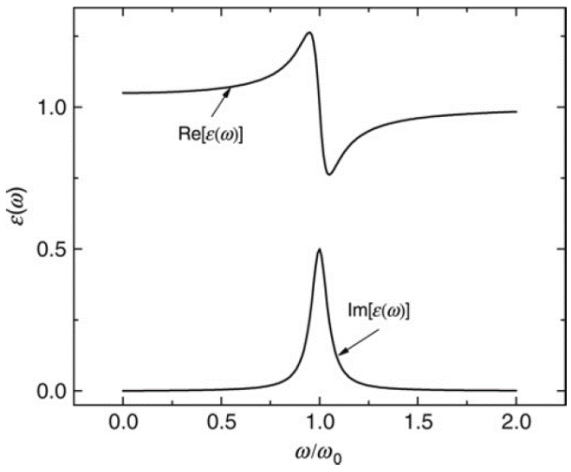

Figure 31: Real and imaginary parts of the complex dielectric function (ϵ(ω)) in and around the resonance frequency (ω0) [3].

We believe our measurements of both extinction and absorption could be used to refine the CRI values of some plastics, especially for the imaginary part in the UV, which other techniques cannot measure accurately. These results are then used as inputs in climate models (alongside the optical properties of many aerosols such as carbon soot), to understand the potential overall impact (warming or cooling) of these aerosols on climate.

Polystyrene: Polystyrene is a common-used kind of plastics due to its characteristics of stiffness. It is used to make products which require the transparence such as food packaging and laboratory supplies. When polystyrene is mixed with colorants, additives or other types of plastics, the combination can make a various range of products in appliances, electronics, household equipment, etc. [47].

Polystyrene beads are used in verification and calibration for the light extinction measurements by the cavity ring down instruments [48].

Measurements: A few works have been conducted to identify microplastics in air and in water. In their master thesis [49], Muhammad Ishaq presented their method for identifying the six common types of microplastics in aquatic environment. The polymers were PP (polypropylene), PS (polystyrene), UPVC (unplasticized polyvinyl chloride), LD-PE (low-density polyethylene), PET (polyethylene terephthalate), PA (polyamide nylon 6) with their thickness range of 0.19-0.55 mm. They used infrared (IR) spectroscopy to extract the IR spectra of the polymers in air and in water. In addition, they also used ellipsometry to derive

the refractive index of the plastics in air. Both methods were promising for the detection of microplastics in water [49].

Besides, measurements of the complex refractive indices of polymers, which is needed for predicting important optical properties, are insufficient, in particular for its imaginary part (sometimes called k) that characterizes the optical absorption. A setup based on spectroscopic ellipsometry (SE) alongside the ray tracing method (RTM) was used for the measurement of the complex refractive indices (CRIs) of five polymers – polydimethylsiloxane, poly(methylmethacrylate) (PMMA), polycarbonate, polystyrene, and the polyethylene terephthalate, in the spectral range of 400-2000 nm [50]. Another method of double optical path length transmission (DOPTM) was applied to measure those characteristics of three polymers - PMMA, polyvinyl chloride, and polyetherimide, in the spectral range of 400-2000 nm [50]. The data showed that the refractive index spectra obtained from both methods approximately matched.

There is a lot of work attempting similar measurements for extracting the CRI of polystyrene, notably in the context of atmospheric aerosol research. The method of integrating vacuum ultraviolet spectroscopy with ellipsometry reported the main peak in absorption at 6.7 eV (185 nm), with a possible shoulder at 5.8 eV (214 nm) [51]. Another technique called Aerosol Extinction Differential Optical Absorption Spectrometer (AE-DOAS) only measured extinction but allowed the derivation of polystyrene's CRI in 220-420 nm [52]. They observed a peak in absorption at approximately 280 nm and below 240/250 nm with large uncertainties. Cavity enhanced spectroscopy with a broadband light source to extract the CRI in wavelength of 360-420 nm showed a small peak in absorption at 410 nm [53]. Nevertheless, they also only measured the extinction of polystyrene. Photoacoustic spectroscopy was applied to measure the absorption but it can only measure at a single wavelength (i.e. 532 nm) [54]. Another technique based on diffuse reflectance and transmittance measurements (integrating sphere) was presented but with a complicated interpretation [55]. It required some assumption on the scattering properties of the medium and Monte-Carlo simulations. The accuracy of the derived CRI depended on the validity of these steps, which could not easily be checked. In addition, they only focused on wavelength larger than 370 nm, for which absorption is negligible.

By measuring the scattering-independent absorption of polystyrene microspheres of different sizes, we aim to characterize more accurately the CRI of polystyrene, especially its imaginary part in the UV, which has not only been measured with other methods suffering from high uncertainties.

3.2. Experimental description

Commercial samples: Five commercial types of spherical polystyrene beads with different size were used. Samples with the diameters of 5 µm, 500 nm, 100 nm, and 78 nm were from Thermo Fisher Scientific [56]. Whereas, the one with the diameter of 2 µm were from Polyscience [57].

Polystyrene measurements: UV Vis spectra – extinction, absorption, and scattering, of microsphere polystyrene with five different diameters - d=5 µm, d=2 µm, d=500 nm, d=100 nm, d=78 nm, were measured by CloudSpec instrument. The spectra were compared with the models – Mie theory calculations.

The aim of our study is not to measure particle size. We use standard highly monodisperse solutions where the size is well-defined. If the complex refractive index (CRI) is known, the measurement of extinction and absorption could be used to derive the size and concentration, but it would not be as accurate as other establishing method such as zeta-sizer or dynamic light scattering.

3.3. Optical properties of polystyrene

Figure 32 shows the extinction, absorption, and scattering spectrum of five types of microsphere polystyrene. We diluted the samples by 100 times except the one with the diameter of 500 nm. It was diluted 800 times due to its saturation of the extinction spectrum at the dilution of 100 times.

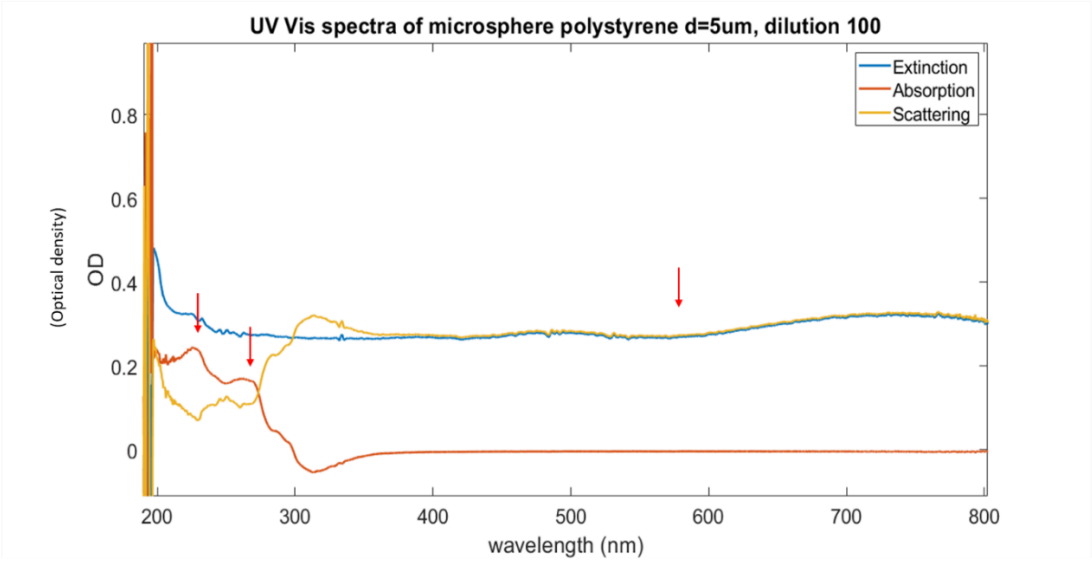

(a)

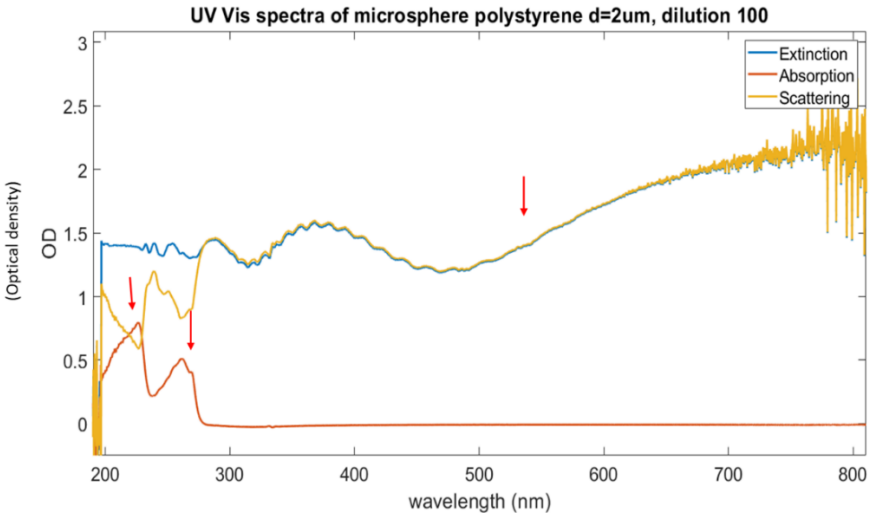

(b)

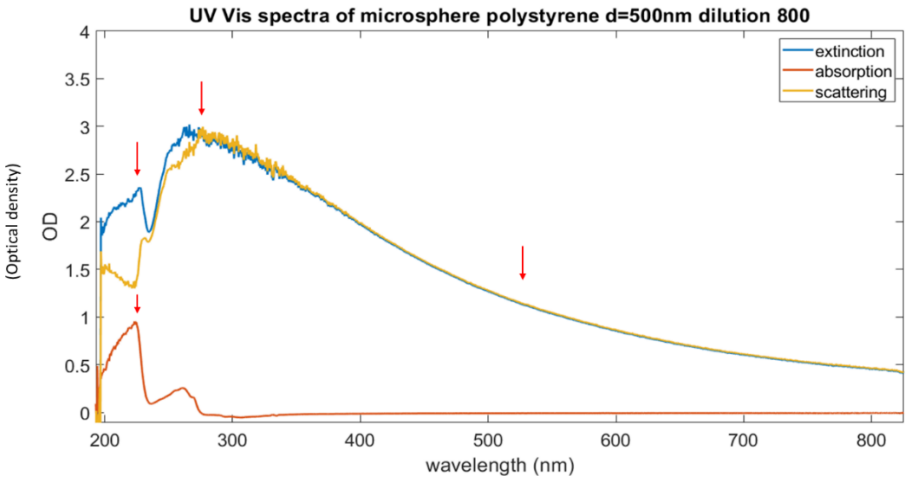
UV Vis spectra of microsphere polystyrene d=500nm dilution 800
extinction
absorption
scattering
(Optical density)
OD
wavelength (nm)

(c)

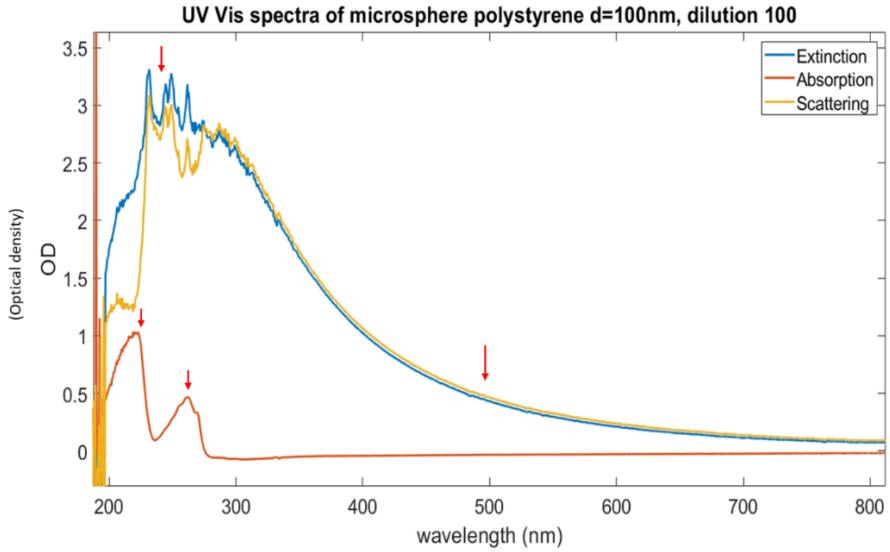
UV Vis spectra of microsphere polystyrene d=100nm, dilution 100
Extinction
Absorption
Scattering
(Optical density)
OD
wavelength (nm)

(d)

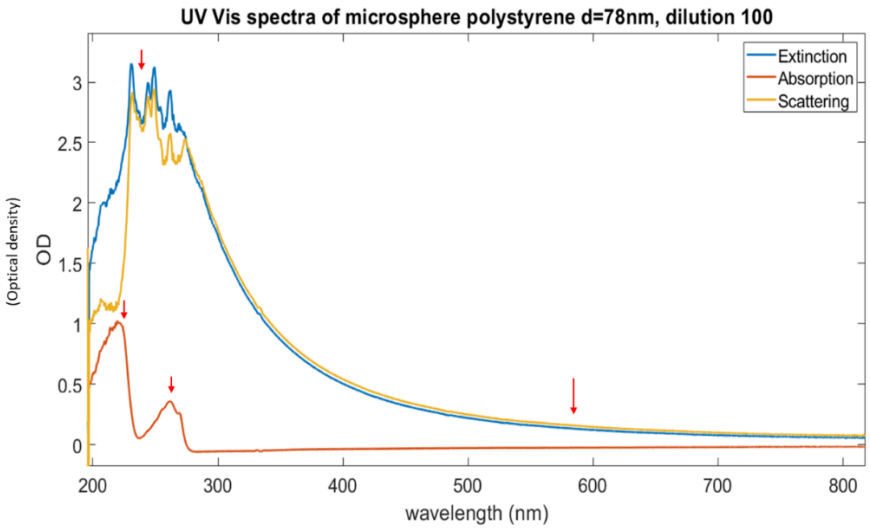

(e)

Figure 32: Ultraviolet and visible spectra of microsphere polystyrene with five different diameters, (a) d=5 µm, (b) d=2 µm, (c) d=500 nm, (d) d=100 nm, and (e) d=78 nm.

As can be seen from the graphs, UV-Vis spectra of the micro sizes – 5 µm and 2 µm had the similarity and those of the nano sizes – 100 nm and 78 nm also had the similar shape. It may come from the fact that the absorption property depends on the chemical structure of the sample whereas the scattering effect has the strong relation with the geometrical characteristics of the sample such as shape and size of the particles.

It is noticeable that there were two absorption maxima in the UV range, i.e. 200-300 nm, for all five samples. While the peaks at the wavelength lower than 240 nm were the sphere's absorption, the other peaks in 240-300 nm should be considered as the absorption of the polymers.

Scattering happened in a wide range of 300-800 nm, that is part of UV spectrum and all visible spectrum.

Another thing is the saturation in UV range of the nano-plastics, i.e. 100 nm and 78 nm. The samples should be diluted more. Also, the minus value was thought to come from the system's error.

3.4. Ultraviolet absorption of polystyrene

Extinction spectra of polystyrene with five diameters (5 µm, 2 µm, 500 nm, 100 nm, 78 nm) measured by CloudSpec were compared with the models. The models are based on Mie theory calculation and programmed by Matlab through SPlaC (SERS and plasmonics codes) [58]. The predicted extinction spectra performed the data in the range of λ=200−900 nm with the standard concentration of 1e-8/100. Extinction spectra of polystyrene samples are compared with those of the models with the reference from refractiveindex.info [59], [60], i.e. the referred dielectric function of polystyrene (ε):

$$\varepsilon = 1 + \frac{1.4435(\lambda_{\mu m})^2}{(\lambda_{\mu m})^2 - 0.020216}$$

, where $\lambda_{\mu m}$ is the wavelength in micrometers.

Figure 33 show the comparison of the experimental spectra and the modeling spectra of the five samples.

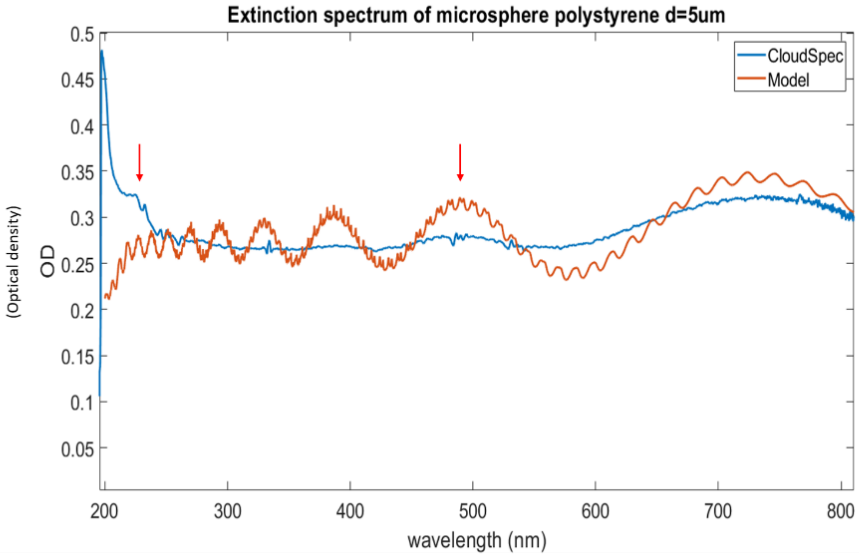
Extinction spectrum of microsphere polystyrene d=5um
CloudSpec
Model
(Optical density)
OD
wavelength (nm)
0.5
0.45
0.4
0.35
0.3
0.25
0.2
0.15
0.1
0.05
200
300
400
500
600
700
800

(a)

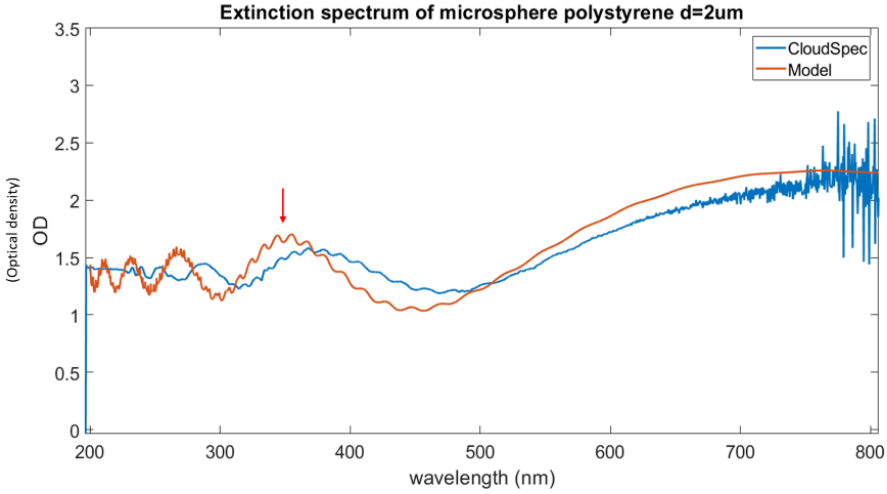
Extinction spectrum of microsphere polystyrene d=2um
CloudSpec
Model
(Optical density)
OD
wavelength (nm)
3.5
3
2.5
2
1.5
1
0.5
0
200
300
400
500
600
700
800

(b)

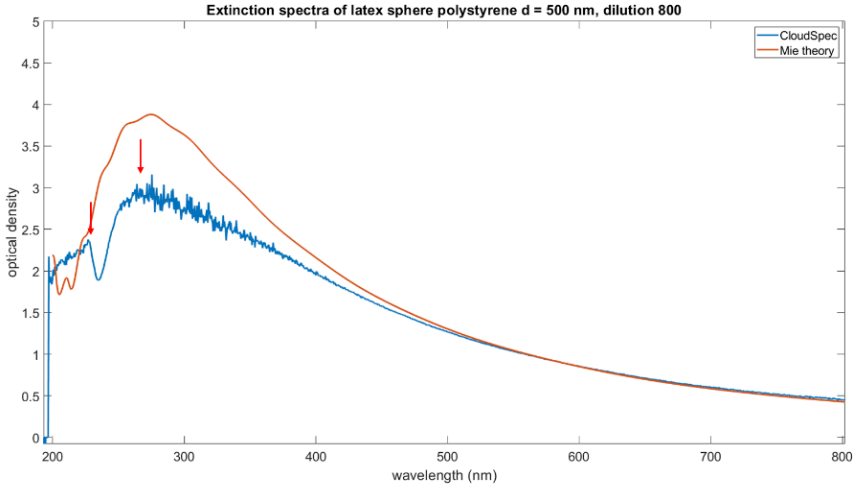
Extinction spectra of latex sphere polystyrene d = 500 nm, dilution 800
CloudSpec
Mie theory
optical density
wavelength (nm)

(c)

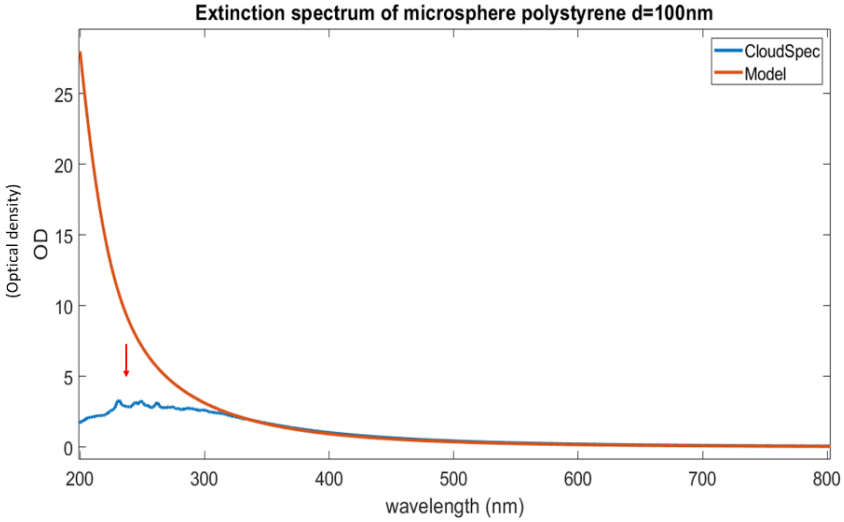
Extinction spectrum of microsphere polystyrene d=100nm
CloudSpec
Model
(Optical density)
OD
wavelength (nm)

(d)

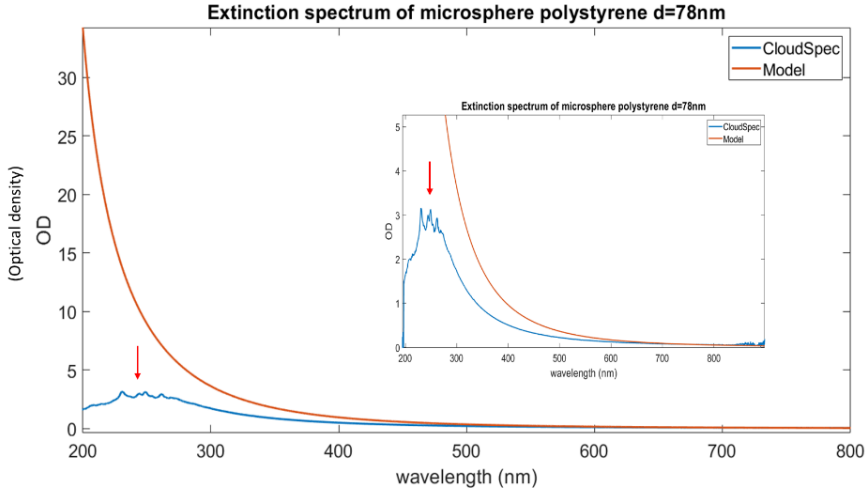
Extinction spectrum of microsphere polystyrene d=78nm
CloudSpec
Model
(Optical density)
OD
wavelength (nm)

(e)

Figure 33: Extinction spectra of microsphere polystyrene with five different diameters measured by CloudSpec in comparison with the models, (a) d=5 µm, (b) d=2 µm, (c) d=500 nm, (d) d=100 nm, and (e) d=78 nm.

The extinction spectra presented their values to be considered in 200-800 nm. The samples were measured by the standard UV-Vis function of CloudSpec which means no usage of the integrating sphere or there was no absorption of the sphere cavity surface in the wavelength smaller than 240 nm like those of the absolute absorption spectra. In comparison with the models, the experimental spectra showed the absorption in UV range which represented the imaginary parts of the complex dielectric function of polystyrene. From the experimental spectra, we can derive useful data which had many applications. As can be seen from the graphs, the modeling spectra with the diameters of 5 µm and 2 µm were similar while those of 100 nm and 78 nm had the same shape. The oscillations or scattering effect of the microsphere - 5 µm and 2 µm depend come from their large sizes. Saturation of the 500-nm sample made its spectrum unmatched with the model.

3.5. Discussion, conclusion and outlook

Our technique appears to provide full absorption/extinction ultraviolet visible spectra of polystyrene in a diameter range of (78 nm, 5 µm) and confirms the peak in k at 280 nm with less sensitivity to large uncertainties and less complication.

In conclusion, the instrument is capable for extracting optical properties, i.e. absorption and scattering, of microplastics. Once the measurements are conducted for the practical samples – polluted air and water, the data could be used to construct climate modeling.

In addition, some electromagnetic modeling, for example using Mie theory, could be applied to derive the concentration of the experimental samples. This would moreover allow one to derive the complex dielectric function (ε) of microsphere polystyrene from our measurements, with useful applications in other fields.

CHAPTER 4 – DISSOLUTION STUDY OF VITAMIN

4.1. Introduction

Vitamins are essential nutrients for human body. Nowadays they are available in form of supplement which also play an important role in health care. There are two groups of vitamin if we consider them in term of solubility, i.e. water-soluble (vitamin B, vitamin C) and oil-soluble (vitamin A, vitamin D, vitamin E). The vitamin supplements can be single or multiple components. In the research, we used effervescence of the complex vitamin B and C with berry flavors which would be prepared by dissolved directly by water.

4.2. Experiment

The idea is to study the time evolution of the spectrum during dissolution of an effervescent tablet of berry-flavoured complex vitamin B and vitamin C supplement (Berocca®) (Figure 34).

Figure 34: The complex vitamin B and vitamin C effervescent tablet (Berocca).

This was done in CloudSpec with the number setting of spectra to 100 in order to have a better time resolution. 1mL water was measured as reference by a 10-mm cuvette. Then we dropped a small amount (a few grains) of the tablet in the cuvette, closed the tower and started a measurement, then restarted as soon as it was finished (approximately every 5.5 seconds).

4.3. Results and discussion

The results are shown below (Figures 35, 36).

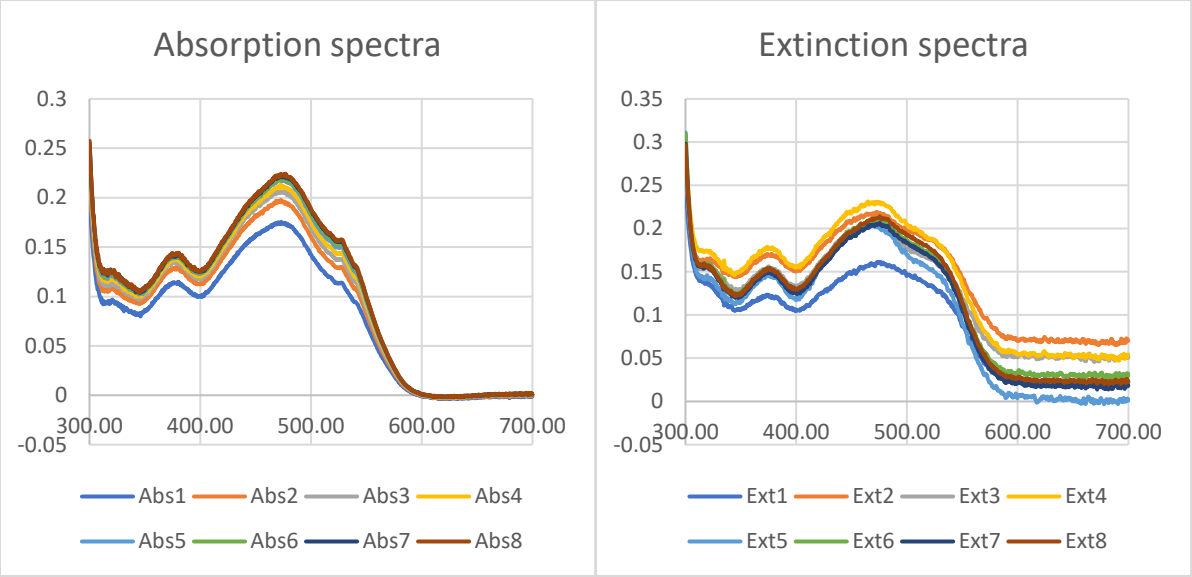

Figure 35: Absorption and extinction spectra of a dissolving effervescent.

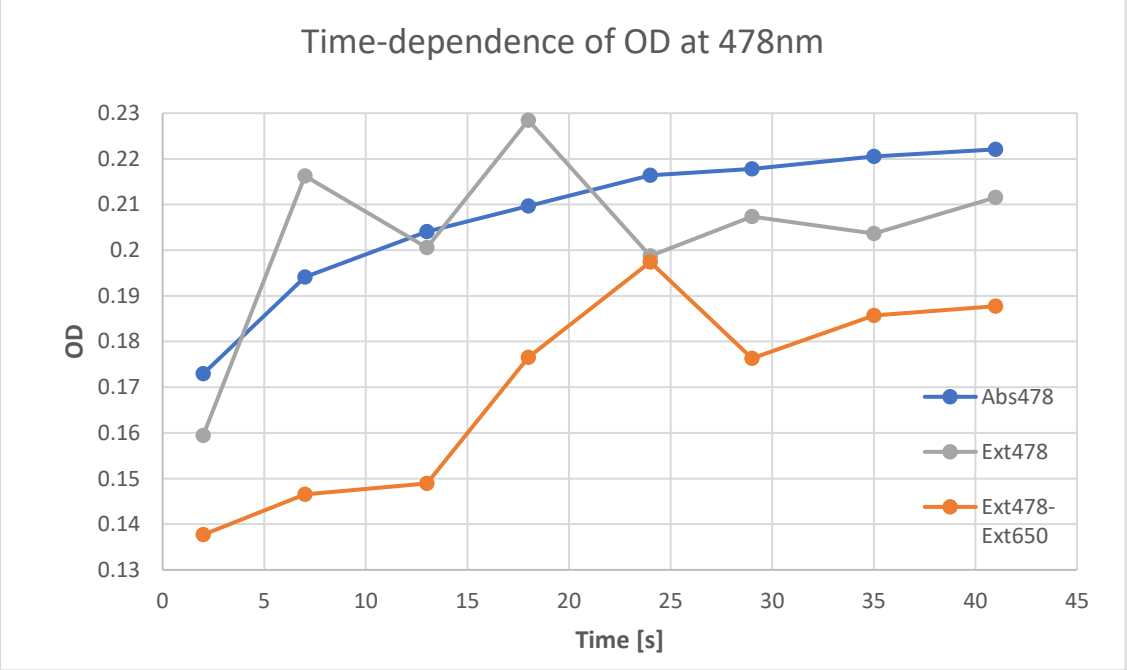

Figure 36: Time-dependence of optical density (OD) of a dissolving effervescent at wavelength of 478 nm.

As expected, the bubbles strongly affect the extinction because of scattering. The presence of bubbles in the extinction beam is random so this creates strong fluctuations. It appears that this cannot be corrected by simple baseline subtraction. In contrast, the absorption increases smoothly and reflects much more reliably the increase in concentration of the active compounds.

CONCLUSION

In conclusion, combined extinction/absorption spectroscopy or CloudSpec can detect essential nutrients, i.e. protein, fat, vitamin A, vitamin B2, in a wide range of commercial milk and cream types. In addition, it is promising in quantifying the nutrients – fat and protein due to the linearity of the absorption in a normal range of their concentration at a number of absorbance maxima whereas the high concentration samples like cream need further study.

The method can extract optical properties, i.e. absorption and scattering, of microplastics with a diameter range of 78 nm – 5 µm. The data can be used to build climate modeling to predict the impact of the plastics on weather or to derive complex dielectric functions of the materials which are useful in many fields. The imaginary part of the dielectric function or ultraviolet absorption of polystyrene which has not been reported yet was observed. Besides, when comparing with the model – Mie theory we can derive the concentration of the samples.

The method is promising in pharmaceutical industry for real-time studying the active agent release in term of effervescent tablets.

BIBLIOGRAPHY

[1] T. Owen, *Fundamentals of UV-visible spectroscopy: A Primer*. 2000.

[2] C. F. Bohren, *Absorption and scattering of light by small particles*. 1983. doi: 10.1088/0031-9112/35/3/025.

[3] E. C. le Ru and P. G. Etchegoin, *Principles of Surface-Enhanced Raman Spectroscopy*. 2009. doi: 10.1016/B978-0-444-52779-0.X0001-3.

[4] X. Wang and Y. Cao, "Characterizations of absorption, scattering, and transmission of typical nanoparticles and their suspensions," *Journal of Industrial and Engineering Chemistry*, vol. 82, 2020, doi: 10.1016/j.jiec.2019.10.030.

[5] Y. Villanueva, C. Veenstra, and W. Steenbergen, "Measuring absorption coefficient of scattering liquids using a tube inside an integrating sphere," *Appl Opt*, vol. 55, no. 11, 2016, doi: 10.1364/ao.55.003030.

[6] E. S. Fry, G. W. Kattawar, and R. M. Pope, "Integrating cavity absorption meter," *Appl Opt*, vol. 31, no. 12, 1992, doi: 10.1364/ao.31.002055.

[7] Brendan Darby, "Probing the interactions between dye molecules and metallic nanoparticles - Implications for surface enhanced spectroscopy," Victoria University of Wellington, Wellington, 2016.

[8] T. Jávorfi *et al.*, "Quantitative spectrophotometry using integrating cavities," *J Photochem Photobiol B*, vol. 82, no. 2, 2006, doi: 10.1016/j.jphotobiol.2005.10.002.

[9] J. T. O. Kirk, "Modeling the performance of an integrating-cavity absorption meter: theory and calculations for a spherical cavity," *Appl Opt*, vol. 34, no. 21, 1995, doi: 10.1364/ao.34.004397.

[10] P. Elterman, "Integrating Cavity Spectroscopy," *Appl Opt*, vol. 9, no. 9, 1970, doi: 10.1364/ao.9.002140.

[11] N. B. Nelson and B. B. Prézelin, "Calibration of an integrating sphere for determining the absorption coefficient of scattering suspensions," *Appl Opt*, vol. 32, no. 33, 1993, doi: 10.1364/ao.32.006710.

[12] M. Babin and D. Stramski, "Light absorption by aquatic particles in the near-infrared spectral region," *Limnol Oceanogr*, vol. 47, no. 3, 2002, doi: 10.4319/lo.2002.47.3.0911.

[13] S. Tassan and G. M. Ferrari, "Variability of light absorption by aquatic particles in the near-infrared spectral region," *Appl Opt*, vol. 42, no. 24, 2003, doi: 10.1364/ao.42.004802.

[14] A. K. Gaigalas, H. J. He, and L. Wang, "Measurement of absorption and scattering with an integrating sphere detector: Application to microalgae," *J Res Natl Inst Stand Technol*, vol. 114, no. 2, 2009, doi: 10.6028/jres.114.006.

[15] D. D. Evanoff and G. Chumanov, "Size-controlled synthesis of nanoparticles. 2. Measurement of extinction, scattering, and absorption cross sections," *Journal of Physical Chemistry B*, vol. 108, no. 37, 2004, doi: 10.1021/jp0475640.

[16] B. L. Darby, B. Auguié, M. Meyer, A. E. Pantoja, and E. C. le Ru, "Modified optical absorption of molecules on metallic nanoparticles at sub-monolayer coverage," *Nat Photonics*, vol. 10, no. 1, 2016, doi: 10.1038/nphoton.2015.205.

[17] V. Petráková, I. C. Sampaio, and S. Reich, "Optical Absorption of Dye Molecules Remains Unaffected by Submonolayer Complex Formation with Metal Nanoparticles," *Journal of Physical Chemistry C*, vol. 123, no. 28, 2019, doi: 10.1021/acs.jpcc.9b05047.

[18] N. R. Larson, Y. Wei, and C. R. Middaugh, "Label-Free, Direct Measurement of Protein Concentrations in Turbid Solutions with a UV-Visible Integrating Cavity Absorbance Spectrometer," *Anal Chem*, vol. 90, no. 8, 2018, doi: 10.1021/acs.analchem.8b00502.

[19] J. Hodgkinson, D. Masiyano, and R. P. Tatam, "Using integrating spheres as absorption cells: Path-length distribution and application of beer's law," *Appl Opt*, vol. 48, no. 30, 2009, doi: 10.1364/AO.48.005748.

[20] C. Tang, M. Meyer, B. L. Darby, B. Auguié, and E. C. le Ru, "Realistic ports in integrating spheres: reflectance, transmittance, and angular redirection," *Appl Opt*, vol. 57, no. 7, 2018, doi: 10.1364/ao.57.001581.

[21] "https://www.cloudspec.co.nz/."

[22] "https://aviantechnologies.com/product/fluorilon-99wtm/."

[23] J. Grand, B. Auguié, and E. C. le Ru, "Combined Extinction and Absorption UV-Visible Spectroscopy as a Method for Revealing Shape Imperfections of Metallic Nanoparticles," *Anal Chem*, vol. 91, no. 22, 2019, doi: 10.1021/acs.analchem.9b03798.

[24] A. Djorović, S. J. Oldenburg, J. Grand, and E. C. le Ru, "Extinction-to-Absorption Ratio for Sensitive Determination of the Size and Dielectric Function of Gold Nanoparticles," *ACS Nano*, vol. 14, no. 12, 2020, doi: 10.1021/acsnano.0c08431.

[25] E. G. Wrigglesworth and J. H. Johnston, "Mie theory and the dichroic effect for spherical gold nanoparticles: an experimental approach," *Nanoscale Adv*, vol. 3, no. 12, 2021, doi: 10.1039/d1na00148e.

[26] C. McGoverin, C. Steed, A. Esan, J. Robertson, S. Swift, and F. Vanholsbeeck, "Optical methods for bacterial detection and characterization," *APL Photonics*, vol. 6, no. 8. 2021. doi: 10.1063/5.0057787.

[27] "http://milkfacts.info/."

[28] A. Gastélum-Barrios, G. M. Soto-Zarazúa, A. Escamilla-García, M. Toledano-Ayala, G. Macías-Bobadilla, and D. Jauregui-Vazquez, "Optical methods based on ultraviolet, visible, and near-infrared spectra to estimate fat and protein in raw milk: A review," *Sensors (Switzerland)*, vol. 20, no. 12. 2020. doi: 10.3390/s20123356.

[29] Andrew Russell, "Milk Spectroscopy," Master Thesis, The University of Waikato, Waikato, New Zealand, 2013.

[30] S. Stocker *et al.*, “Broadband Optical Properties of Milk,” *Appl Spectrosc*, vol. 71, no. 5, 2017, doi: 10.1177/0003702816666289.

[31] S. Xiong, B. Adhikari, X. D. Chen, and L. Che, “Determination of ultra-low milk fat content using dual-wavelength ultraviolet spectroscopy,” *J Dairy Sci*, vol. 99, no. 12, 2016, doi: 10.3168/jds.2016-11640.

[32] R. Stefanescu, S. Brebu, M. Matei, I. M. Risca, A. Surleva, and G. Drochioiu, “Contribution to Casein Determination by UV Spectrophotometry,” *Acta Chemica Iasi*, vol. 25, no. 2, 2017, doi: 10.1515/achi-2017-0011.

[33] “https://www.azom.com/article.aspx?ArticleID=13760.”

[34] A. Gowri, A. S. Rajamani, B. Ramakrishna, and V. V. R. Sai, “U-bent plastic optical fiber probes as refractive index based fat sensor for milk quality monitoring,” *Optical Fiber Technology*, vol. 47, 2019, doi: 10.1016/j.yofte.2018.11.019.

[35] F. Fohely and N. Suardi, “Study the Characterization of Spectral Absorbance on Irradiated Milk Protein,” in *Journal of Physics: Conference Series*, 2018, vol. 995, no. 1. doi: 10.1088/1742-6596/995/1/012056.

[36] R. A. Morton and I. M. Heilbron, “The absorption spectrum of vitamin A [1],” *Nature*, vol. 122, no. 3062. 1928. doi: 10.1038/122010a0.

[37] R. Bartzatt and T. Wol, “Detection and Assay of Vitamin B-2 (Riboflavin) in Alkaline Borate Buffer with UV/Visible Spectrophotometry,” *Int Sch Res Notices*, vol. 2014, 2014, doi: 10.1155/2014/453085.

[38] P. Pokale, S. Shende, A. Gade, and M. Rai, “Biofabrication of calcium phosphate nanoparticles using the plant Mimusops elengi,” *Environ Chem Lett*, vol. 12, no. 3, 2014, doi: 10.1007/s10311-014-0460-8.

[39] L. Cai *et al.*, “Characteristic of microplastics in the atmospheric fallout from Dongguan city, China: preliminary research and first evidence,” *Environmental Science and Pollution Research*, vol. 24, no. 32, 2017, doi: 10.1007/s11356-017-0116-x.

[40] S. Allen *et al.*, “Atmospheric transport and deposition of microplastics in a remote mountain catchment,” *Nat Geosci*, vol. 12, no. 5, 2019, doi: 10.1038/s41561-019-0335-5.

[41] S. Dehghani, F. Moore, and R. Akhbarizadeh, “Microplastic pollution in deposited urban dust, Tehran metropolis, Iran,” *Environmental Science and Pollution Research*, vol. 24, no. 25, 2017, doi: 10.1007/s11356-017-9674-1.

[42] A. A. Horton and S. J. Dixon, “Microplastics: An introduction to environmental transport processes,” *WIREs Water*, vol. 5, no. 2, 2018, doi: 10.1002/wat2.1268.

[43] M. Wu *et al.*, “Impacts of Aerosol Dry Deposition on Black Carbon Spatial Distributions and Radiative Effects in the Community Atmosphere Model CAM5,” *J Adv Model Earth Syst*, vol. 10, no. 5, 2018, doi: 10.1029/2017MS001219.

[44] L. E. Revell, P. Kuma, E. C. le Ru, W. R. C. Somerville, and S. Gaw, “Direct radiative effects of airborne microplastics,” *Nature*, vol. 598, no. 7881, 2021, doi: 10.1038/s41586-021-03864-x.

[45] U. of C. Laura Revell, “The IPCC AR5 Working Group 1 report.”

[46] U. of C. Laura Revell, “Microplastics Research Proposal.”

[47] “https://www.chemicalsafetyfacts.org/polystyrene/.”

[48] R. E. H. Miles, S. Rudić, A. J. Orr-Ewing, and J. P. Reid, “Influence of uncertainties in the diameter and refractive index of calibration polystyrene beads on the retrieval of aerosol optical properties using cavity ring down spectroscopy,” *Journal of Physical Chemistry A*, vol. 114, no. 26, 2010, doi: 10.1021/jp103246t.

[49] Muhammad Umair Ishaq, “On optical properties of transparent micro- and nanoplastics,” Master Thesis, University of Eastern Finland, 2019.

[50] X. Zhang, J. Qiu, X. Li, J. Zhao, and L. Liu, “Complex refractive indices measurements of polymers in visible and near-infrared bands,” *Appl Opt*, vol. 59, no. 8, 2020, doi: 10.1364/ao.383831.

[51] R. H. French, K. I. Winey, M. K. Yang, and W. Qiu, “Optical properties and van der Waals-London dispersion interactions of polystyrene determined by vacuum ultraviolet spectroscopy and spectroscopic ellipsometry,” *Aust J Chem*, vol. 60, no. 4, 2007, doi: 10.1071/CH06222.

[52] T. Galpin, R. T. Chartier, N. Levergood, and M. E. Greenslade, “Refractive index retrievals for polystyrene latex spheres in the spectral range 220–420 nm,” *Aerosol Science and Technology*, vol. 51, no. 10, 2017, doi: 10.1080/02786826.2017.1339014.

[53] R. A. Washenfelder, J. M. Flores, C. A. Brock, S. S. Brown, and Y. Rudich, “Broadband measurements of aerosol extinction in the ultraviolet spectral region,” *Atmos Meas Tech*, vol. 6, no. 4, 2013, doi: 10.5194/amt-6-861-2013.

[54] D. A. Lack, E. R. Lovejoy, T. Baynard, A. Pettersson, and A. R. Ravishankara, “Aerosol Absorption Measurement using Photoacoustic Spectroscopy: Sensitivity, Calibration, and Uncertainty Developments,” *Aerosol Science and Technology*, vol. 40, no. 9, 2006, doi: 10.1080/02786820600803917.

[55] X. Ma, J. Q. Lu, R. S. Brock, K. M. Jacobs, P. Yang, and X. H. Hu, “Determination of complex refractive index of polystyrene microspheres from 370 to 1610 nm,” *Phys Med Biol*, vol. 48, no. 24, 2003, doi: 10.1088/0031-9155/48/24/013.

[56] “https://www.thermofisher.com/.”

[57] “https://www.polysciences.com/.”

[58] “https://www.wgtn.ac.nz/scps/research/research-groups/raman-lab.”

[59] “https://refractiveindex.info/?shelf=organic&book=polystyren&page=Sultanova.”

[60] N. Sultanova, S. Kasarova, and I. Nikolov, “Dispersion properties of optical polymers,” in *Acta Physica Polonica A*, 2009, vol. 116, no. 4. doi: 10.12693/APhysPolA.116.585.